

### 3. SAND PROVENANCE IN THE ALBORAN AND TYRRHENIAN BASINS<sup>1</sup>

Kathleen M. Marsaglia,<sup>2</sup> Kelly K. Latter,<sup>3</sup> and Veronica Cline<sup>3</sup>

#### ABSTRACT

Miocene to Pleistocene sand and sandstone were recovered at Ocean Drilling Program Site 974 in the Tyrrhenian Basin and Sites 976 and 977 in the Alboran Basin. Sand detrital modes were determined for 45 samples from these sites, as well as 10 samples of Spanish beach sand. At Site 974, the Pleistocene section includes a number of volcaniclastic (vitric ash) and terrigenous sand layers; the latter are heterogeneous and contain sedimentary and metamorphic lithic fragments. Submarine canyon and onshore drainage patterns suggest that the most likely source of this sediment is the Tiber River drainage basin in central Italy, where a Pleistocene volcanic field is superimposed on Apennine orogenic rocks. In contrast, the Miocene sand in Unit III at Site 974 may have been derived from local basement highs. The quartzolitic composition and preponderance of metamorphic and sedimentary lithic debris in sand samples from Unit II at Site 976, Unit I at Sites 977 and 978, and Unit I at Site 979 are consistent with derivation from metamorphic rocks and sedimentary cover sequences that crop out in the Betic Cordillera of southern Spain (976–978) and in the Rif of Northern Africa (979). The sedimentary to metamorphic lithic fragment ratios in these samples reflect the relative proportion of metamorphic and sedimentary rocks exposed in onshore source terranes. In contrast, the source of the few quartzose Pleistocene sands at Site 976 was likely the Flysch Trough Units that crop out near Gibraltar. The significant volcanic component in certain intervals at Sites 976 (upper Miocene) and 977 (lower Pliocene to Miocene) is consistent with widespread volcanic activity during basin inception and development. Mean sand detrital modes for sand subgroups from both the Alboran and Tyrrhenian Basin sites plot in the Recycled Orogenic and Magmatic Arc compositional fields of Dickinson et al. (1983), reflecting the hybrid tectonic histories of these basins.

#### INTRODUCTION

##### Geologic Background

The Alboran and Tyrrhenian Seas are tectonically active, postcollisional basins that are located in the broad region of deformation that marks the modern African and European plate boundary (Fig. 1). These basins are superimposed on the Alpine orogenic belt and are both characterized by extension and magmatism.

The Tyrrhenian Sea (Fig. 2) is a “Mediterranean backarc basin” that initiated during the Miocene behind the Eolian-Calabrian calc-alkaline magmatic arc in conjunction with lithospheric subduction and marginal compression (Beccaluva et al., 1990; Jolivet et al., 1994; Kastens and Mascle, 1990; Mantovani et al., 1996; Rehault et al., 1987a, 1987b; Selli, 1985; Wezel, 1985). It is partly surrounded by Alpine orogenic chains, and floored along its margins by extended continental crust and in its center by young oceanic-type crust (Rehault et al., 1987a, 1987b; Beccaluva et al., 1990).

In contrast, the Alboran Basin is mostly surrounded by the Betic and Rif orogenic chains (Figs. 1, 3), is floored entirely by extended continental crust, and is more tectonically complex with a history that includes rifting from the Aquitanian to early Tortonian, and postrift compression and strike-slip faulting and folding from the late Tortonian onwards (Buforn et al., 1995; Comas et al., 1992; Fernandez and Sanz de Galdeano, 1992; Horvath and Berckhemer, 1982; Morel and Meghraoui, 1996; Platt and Vissers, 1989). Extension was associated with calc-alkaline to felsic magmatism, whereas later compression was associated with calc-alkaline to alkaline magmatism (Bellon et al., 1983; Comas et al., 1992; Comas, Zahn, Klaus, et al., 1996; Hernandez et al., 1987). Unlike the Tyrrhenian Sea, however, the Albo-

ran Sea shows no clear evidence for subduction of oceanic lithosphere during its evolution (Comas, Zahn, Klaus, et al., 1996). The Betic and Rif mountain chains comprise the Alboran Domain, which is mainly composed of metamorphic complexes and is thought to constitute the basement below the Alboran Sea (Comas, Zahn, Klaus, et al., 1996, and references therein; Garcia-Dueñas et al., 1992).

##### Drilling Results

One purpose of Ocean Drilling Program (ODP) Leg 161 was to characterize and compare the depositional histories of the various sub-basins of the Western Mediterranean (Comas, Zahn, Klaus, et al., 1996). During this leg, Site 974 was drilled in the Tyrrhenian Sea and Sites 976–979 were drilled in the Alboran Sea (Fig. 1).

Site 974 is located in the central part of the Tyrrhenian Sea along the Sardinian passive continental margin (Fig. 2). It sits in a north trending, elongate slope basin that is a half graben underlain by a small fault-bounded block of thinned continental crust (Kastens, Mascle, Auroux, et al., 1987). The sedimentary sequence recovered at Site 974 was divided into three lithostratigraphic units by shipboard scientists (Fig. 4; Comas, Zahn, Klaus, et al., 1996). Unit I consists predominantly of Pleistocene to Pliocene nannofossil-rich clay to silty clay with minor ash/sand and organic-rich layers. It is underlain by Pliocene nannofossil clay and ooze with minor altered-ash and organic-rich layers (Unit II). The basal Unit III consists of Miocene clay, calcareous silty clay, silt, and sand.

Site 976, the westernmost site in the Alboran Sea (Fig. 3), is located on a metamorphic basement high covered by Pleistocene through Miocene sediments (Comas et al., 1996). The stratigraphy at Site 976 was divided by shipboard scientists into five lithologic units (Fig. 4). Unit I is predominantly composed of Pleistocene to late Pliocene nannofossil clay to silty clay to clay with minor sandy silt layers. Unit II is late Pliocene in age, with poor recovery characterized by unconsolidated sand, carbonate-cemented sandstone, and nannofossil clay. Early late Pliocene to middle Miocene nannofossil clay and claystone are the dominant lithologies in Unit III. The basal Unit IV is a thin interval of middle Miocene sand and pebbly sand overlying the metamorphic basement of Unit V.

<sup>1</sup>Zahn, R., Comas, M.C., and Klaus, A. (Eds.), 1999. *Proc. ODP, Sci. Results*, 161: College Station, TX (Ocean Drilling Program).

<sup>2</sup>Dept. of Geological and Environmental Sciences, Stanford University, Stanford, CA 94305, U.S.A. (Present address: Westport, 6700 Portwest Drive, Houston, TX 77024, U.S.A.) marsaglia@ibm.net

<sup>3</sup>Dept. of Geological and Environmental Sciences, University of Texas at El Paso, El Paso, TX 79968, U.S.A.

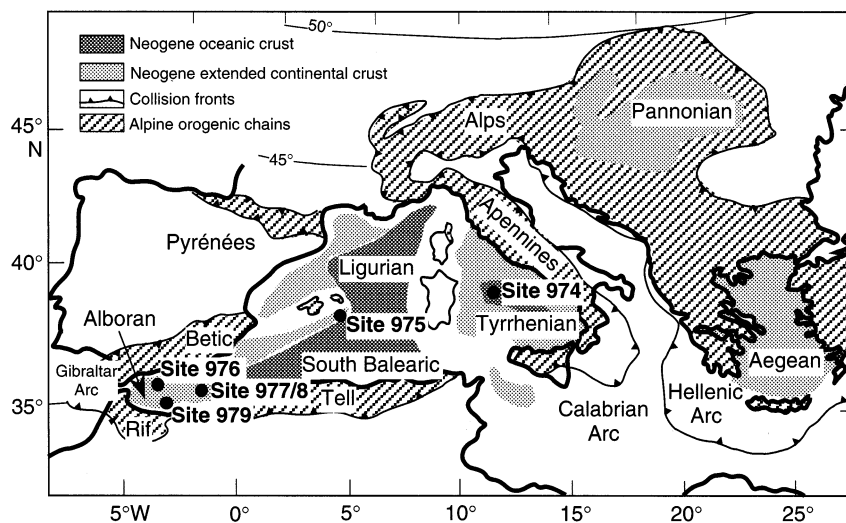


Figure 1. Map showing the distribution of Alpine orogenic chains, collision fronts, basins floored by extended continental crust and oceanic crust (Alboran, Ligurian, South Balearic, Tyrrhenian, Pannonian, and Aegean), and Leg 161 drill sites. From Comas, Zahn, Klaus, et al. (1996).

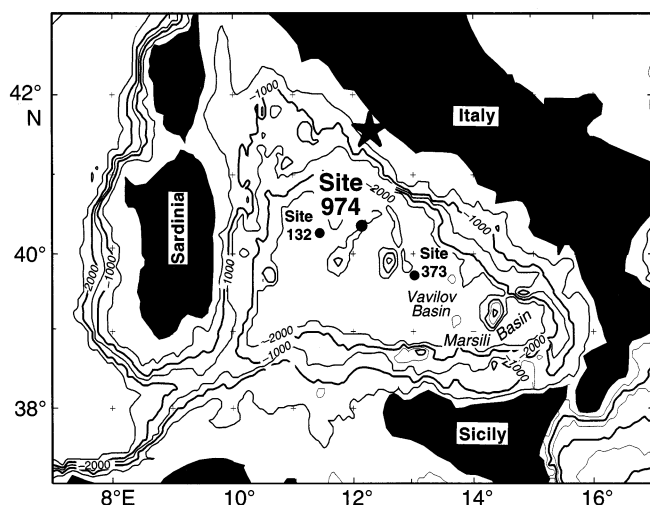


Figure 2. Map of Tyrrhenian Sea with the location of ODP Site 974 and DSDP sites. Star marks the approximate position of Tiber River delta along coast of Italy. Contours are in mbsl. Modified from Comas, Zahn, Klaus, et al. (1996).

Sites 977 and 978 are located in the Eastern Alboran Basin, a 35-km-wide graben that is roughly equidistant from the Spanish and North African coasts (Fig. 3). The sites lie north and south, respectively, of the Al-Mansour Seamount, a volcanic high that subdivides the basin (Fig. 3). The sequence cored at Site 977 was divided into two lithostratigraphic units by shipboard scientists (Fig. 4): Unit I consists of Pliocene–Pleistocene nannofossil clay and nannofossil-rich silty clay with sparse sandy layers, and Unit II consists of partly cemented gravel that is Early Pliocene to Miocene(?) in age. The lithostratigraphy at Site 978 is similar to that at Site 977 (Fig. 4), but shipboard scientists divided Unit I into three subunits, based in part on the presence of cyclic dark-light intervals. In addition, the gravel of Unit II was completely penetrated at Site 978, below which a sequence of late Miocene claystone, siltstone, and sandstone (Unit III) was recovered.

Site 979 is situated in the Southern Alboran Basin, between the Alboran Ridge and the coast of North Africa (Fig. 3). A single lithostratigraphic unit was penetrated at this site (Fig. 4), consisting predominantly of nannofossil clay with minor sand and silt layers.

Although a number of sites were drilled in the Tyrrhenian and Alboran Seas during previous legs of the Deep Sea Drilling Project

(DSDP) and Ocean Drilling Program (ODP), to our knowledge, no detrital modes were determined for sand recovered at these sites (i.e., Sites 121, 132, 373, 650–656) except for the Miocene of the Tyrrhenian Basin (Borsetti et al., 1990). For this study, we sampled sand-bearing cores from Sites 974, 976, 977, 978, and 979 and petrographically analyzed the samples to: (1) outline the compositional variation and determine the likely provenance of Miocene through Pleistocene sand deposited at Leg 161 sites in the Alboran and Tyrrhenian Seas; (2) relate sand detrital modes to the tectonic evolution of each region; and (3) compare and contrast Alboran and Tyrrhenian sand detrital modes with those reported in the literature for other basins. Herein we also present compositional results for onshore sand samples that were collected from the southern Spanish coast (Fig. 5) in order to better constrain Site 976, 977, and 978 sand provenance. Note that the petrology and provenance of Miocene sandy intervals at Site 975 in the South Balearic Basin (Figs. 1, 4) are addressed elsewhere in this volume (Marsaglia and Tribble, Chap. 1, this volume).

## METHODS

One hundred seventy-eight samples of sandstone and loose sand were collected from Leg 161 cores for this study: 13 from Site 974, 40 from Site 976, 41 from Site 977, 42 from Site 978 and 42 from Site 979. Based on their textures and sedimentary structures, these sandy layers were interpreted by shipboard scientists (Comas, Zahn, Klaus, et al., 1996) as turbidites (Sites 975, 976, 977, 978, and 979) and possibly contourites (Sites 977 and 978). An additional 10 samples were collected from beaches along the southern Spanish coast including sites at or near the mouths of major rivers (Fig. 5; see Latter [1998]).

The loose samples were air dried and then sieved to obtain the sand-sized fraction (0.0625–2.0 mm). Semi-indurated and indurated sandstone chips were vacuum impregnated with blue-dyed epoxy. Thin sections prepared from the loose samples and chips were stained for the recognition of potassium and calcium feldspar using the method outlined in Marsaglia and Tazaki (1992).

All the thin sections were first petrographically examined to determine if they contain sufficient sand-sized terrigenous grains for point-counting. Unfortunately, most of the Leg 161 samples collected for this study were unsuitable because they either contained insufficient sand-sized material, or consisted mainly of bioclastic debris (see Latter [1998] for detailed listing of sample intervals). Therefore, sand detrital modes were determined for only 11 samples from Site 974, 13 samples from Site 976, 8 samples from Site 977, 3 samples from Site 978, and 10 samples from Site 979. We used the Gazzi-Dickinson method of point counting, which minimizes the effects of

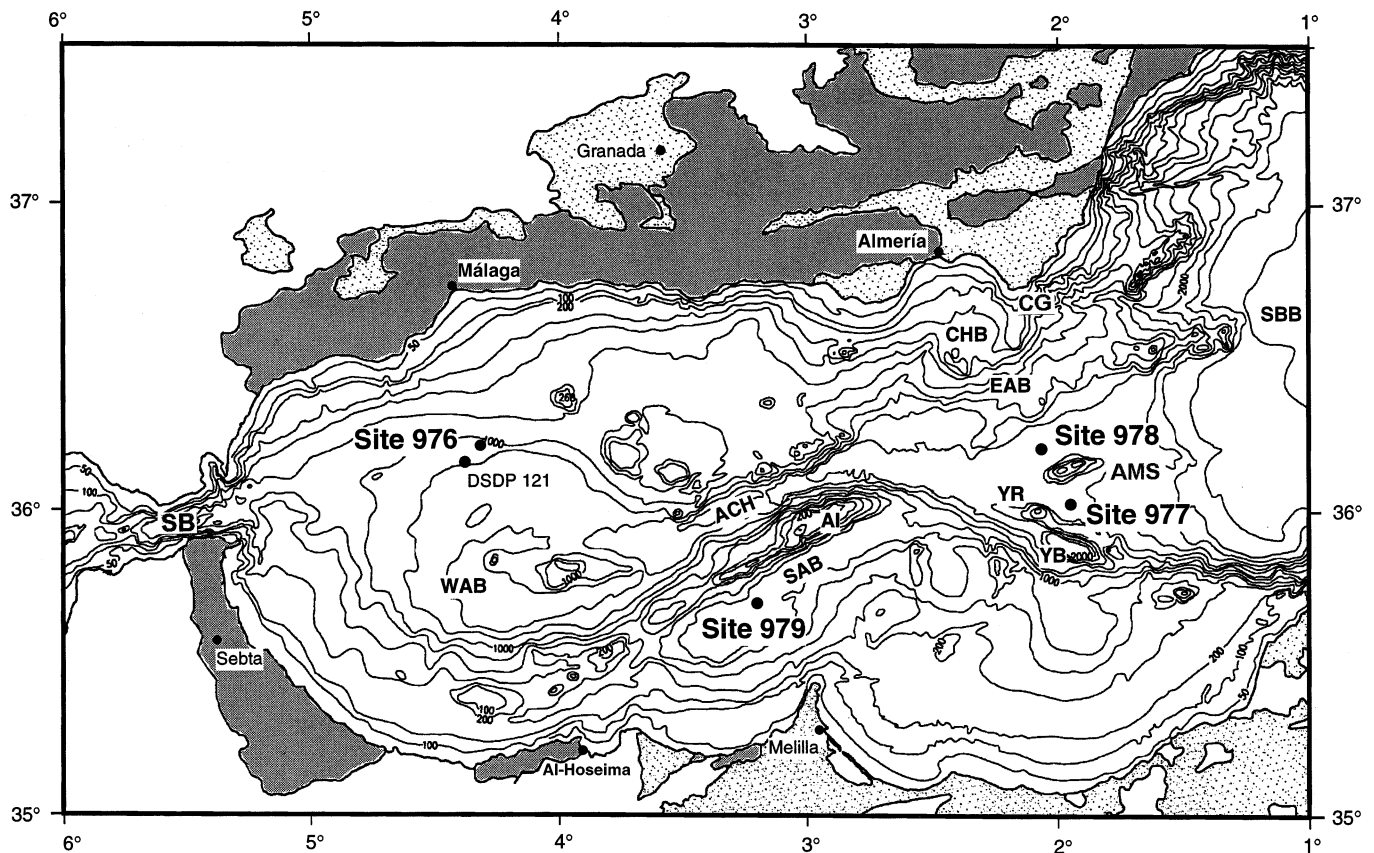


Figure 3. Bathymetry of Alboran Sea with Leg 161 site locations and onshore distribution of Miocene marine sediments (dotted pattern), and Alboran Domain rocks (gray). Contours are in mbsl. SB = Strait of Gibraltar; WAB = West Alboran Basin; ACH = Alboran Channel (Alboran Trough); SAB = South Alboran Basin; AI = Alboran Island (on Alboran Ridge); YR = Yusuf Ridge; YB = Yusuf Basin; AMS = Al-Mansour Seamount; EAB = Eastern Alboran Basin; CHB = Chella Bank; CG = Cabo de Gata; SBB = South Balearic Basin. From Comas, Zahn, Klaus, et al. (1996).

grain-size variation on composition (Dickinson, 1970; Ingersoll et al., 1984). The use of this method is important because of the wide range in sample grain size, from very fine to coarse sand. Multiple monomineralic and lithic categories of grains were distinguished with lithic fragments further subdivided according to texture and mineralogy (Table 1), using schemes outlined in Dickinson (1970), Dickinson et al. (1983), and Marsaglia and Ingersoll (1992). Up to four hundred points were counted per thin section, with the total depending on sand grain size and concentration (Table 2). Recalculated parameters for these data (Tables 1, 2) were used to construct ternary plots. Note that bioclasts were not counted in all samples.

## PETROGRAPHIC DESCRIPTIONS

### Site 974

Unit I sand layers fall into two compositional groups. The first group consists of volcanoclastic (ash) layers (Cores 161-974B-3H, 7H, and 9H) that are predominantly composed of colorless vitric bubble-wall and pumice fragments; these stain according to their composition and range from uniformly yellow (K-rich) or pink (Ca-rich) to a mixture of both (Ca- and K-bearing). The other samples from Unit I (Cores 974B-1H, 2H, 4H, 5H, and 6H) constitute the second group, and these are predominantly composed of monocrystalline quartz, plagioclase and potassium feldspar grains, and metamorphic lithic fragments. The latter consist of quartz-mica tectonite with lesser polycrystalline mica and quartz-feldspar-mica aggregates (Pl. 1). The youngest sample (974B-1H-3, 139–140 cm) from this second group contains more volcanic lithic fragments (brown microlitic glass and

pumice with calcium and potassium stain; Pl. 1) and a wider variety of dense minerals including green amphibole, olivine(?), apatite, garnet, tourmaline, and sphene. Sedimentary lithic fragments in two samples (Cores 974B-1H-3, 139–140 cm and 2H-4, 63–65 cm) are a mix of argillite (Lsa) and limestone (Lsc) debris (Pl. 1).

Of the three samples from Unit III, one, the coarsest (161-974B-22X-CC, 28–29 cm), has a modal composition that is very similar to Unit I sand. In addition to monocrystalline and polycrystalline quartz, plagioclase and potassium feldspar grains, this sample contains fragments of granite (plagioclase + potassium feldspar + quartz + biotite), gneiss and/or coarse schist (biotite + quartz; Pl. 1), quartz-mica tectonite, siltstone, sedimentary carbonate (foraminifer calcarenite, foraminifer microsparite, and dolosiltite), and altered and devitrified felsic to intermediate to mafic volcanic debris. Many of the coarse-grained lithic fragments were included in monomineralic categories during point counting (function of Gazzi-Dickinson method). The other Unit III samples are quartzo-lithic with primarily sedimentary and lesser metamorphic lithics.

### Site 976

In sand from Units I, II and III at Site 976, quartz is abundant as singular grains, and as sand-sized crystals in quartz-mica tectonite fragments. It commonly exhibits undulatory extinction (Pl. 2). Grains of plagioclase, potassium feldspar, and mica flakes (biotite, muscovite, and chlorite) are also common monomineralic components. Biotite is locally altered to opaques and chlorite, and plagioclase ranges from fresh to altered. Rare grains of polycrystalline quartz are present. Within the lithic fraction, metamorphic lithic fragments are

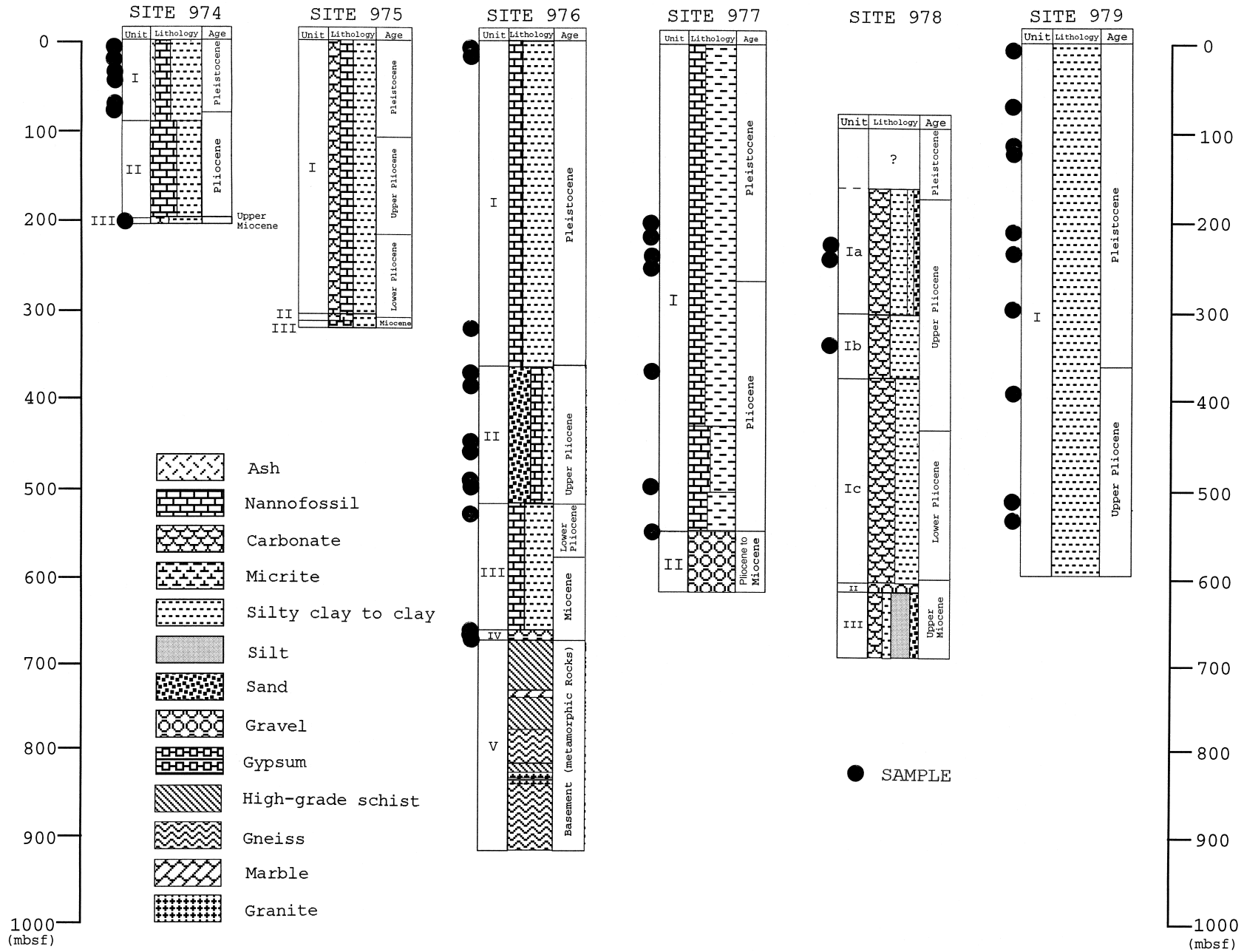


Figure 4. Representative stratigraphic columns for Leg 161 sites. See Marsaglia and Tribble (Chap. 1, this volume) for discussion of Miocene sand composition at Site 974. Locations of point-counted samples indicated by dots on side of columns. From Comas, Zahn, Klaus, et al. (1996).

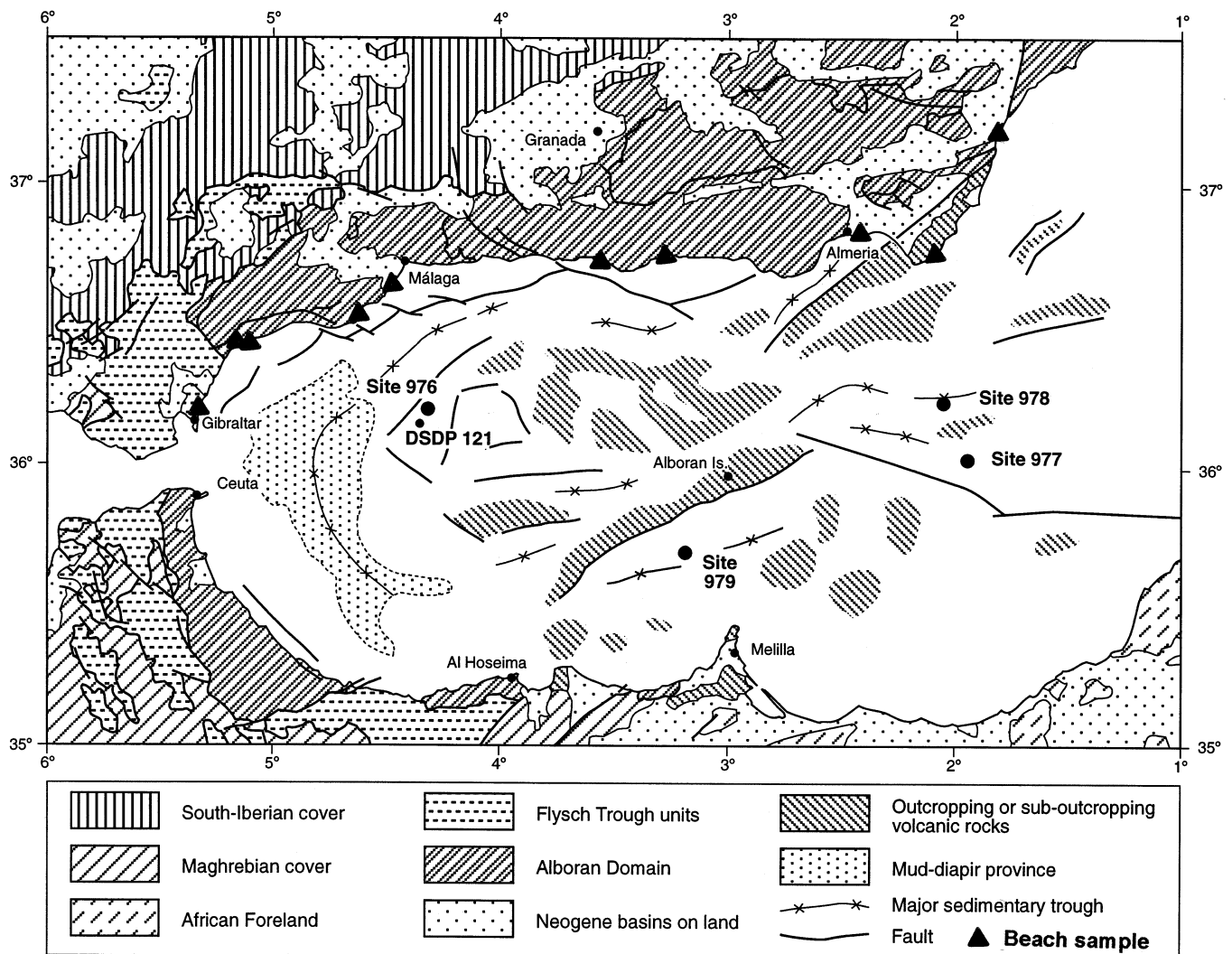


Figure 5. Generalized geological and structural map of the Alboran Sea with DSDP (121) and ODP (976–979) site locations. From Comas, Zahn, Klaus, et al. (1996).

the most common. They are predominantly quartz-mica tectonite (Lmt), locally graphitic, with lesser polycrystalline mica (Lmm), serpentinite (Lmv), and phyllite (Pl. 2). Sedimentary lithic fragments include shale/argillite (Lsa) and carbonate (Lsc) lithic fragments. It is possible that some fragments counted as carbonate lithic clasts could be bioclastic debris. Both unconsolidated sand and carbonate-cemented sandstone samples were collected from Unit II; these contain a variety of carbonate components such as bioclasts, carbonate sedimentary lithic fragments, marble metamorphic lithic fragments (coarse carbonate), and incipient (coarse carbonate crystals in loose samples) to pervasive (in sandstone samples) authigenic carbonate cement. The detrital vs. authigenic (incipient cementation) origin of sand-sized carbonate was most easily determined in the cemented samples of Unit II; for that reason, mainly carbonate-cemented samples were analyzed from this unit (Pl. 2; Table 2).

Although shipboard scientists noted the unusual texture and presence of phillipsite in Unit IV sediments at Site 976 (Comas, Zahn, Klaus, et al., 1996), it was not until thin sections were prepared for this study that relict volcanoclastic textures were recognized in this unit. Unfortunately, samples from Unit IV were dried, disaggregated, and sieved; had they been first impregnated with epoxy, the extent of volcanic grain dissolution and alteration, and thus the original percentage of volcanic debris in the deposit, would have been more eas-

ily constrained. As seen in thin section, the sand-sized fraction includes clumps or “gloms” of sandy matrix that contain silt-sized fragments of volcanic glass completely altered to green clay minerals; these “gloms” also provide some textural evidence to suggest that there has been dissolution of volcanic glass and plagioclase phenocrysts (secondary porosity) and replacement/cementation by zeolites. The major sand-sized components in the three samples from Unit IV are quartz, feldspar, and authigenic zeolites. Given the propensity for feldspar and zeolite to stain, some feldspar grains may have been inadvertently counted as zeolite and visa versa. Only a few percent of sand-sized volcanic lithic debris was recognizable, including felsitic, microlitic, and vitric (pumice and shard) varieties (Pl. 2) with plagioclase phenocrysts (often partly to wholly altered). The vitric groundmass of these fragments is completely altered to green clay minerals. Euhedral to embayed biotite crystals are also present. Although no volcanic lithic fragments were identified in Sample 161-976B-72X-2, 52–54 cm, the high proportion of plagioclase feldspar crystals (phenocrysts?) and secondary zeolite in this sample suggest that it may have also had a volcanoclastic component. Metamorphic lithic fragments are also common components of Unit IV sands, but many of the coarser fragments (e.g., coarse schist; Pl. 2) were counted in monomineralic categories. Unit IV sand also contains a minor percentage of glauconite.

**Table 1. Counted and recalculated parameters.**

Counted Parameters:		Recalculated Parameters
Qp:	Polycrystalline quartz	$QFL\%Q = 100*Q/(Q + F + L)$
Qm:	Monocrystalline quartz	$QFL\%F = 100*F/(Q + F + L)$
P:	Plagioclase feldspar	$QFL\%L = 100*L/(Q + F + L)$
Palt zeol:	Plagioclase altered to zeolite	
Funst:	Unstained (Na?) feldspar	$QmKP\%Qm = 100*Qm/(Qm + P + Fu)$
K:	Potassium feldspar	$QmKP\%P = 100*(P + Fu)/(Qm + P + Fu)$
Lvf:	Felsitic volcanic	$QmKP\%K = 100*K/(Qm + P + Fu)$
Lvv:	Vitric volcanic lithic	
Lvml:	Microplitic volcanic lithic	$LmLvLs\%Lm = 100*Lm/L$
Lvl:	Lathwork volcanic lithic	$LmLvLs\%Lv = 100*Lv/L$
Lmv Serp:	Serpentine	$LmLvLs\%Ls = 100*Ls/L$
Lmm:	Polycrystalline mica lithic	
Lmt:	Quartz-mica tectonite (schist) lithic	$QmFLt\%Qm = 100*Qm/(Q+F+L)$
Lma:	Quartz-feldspar-mica aggregate lithic	$QmFLt\%F = 100*F/(Q+F+L)$
Lmp:	Phyllite lithic	$QmFLt\%Lt = 100*(L+Qp)/(Q+F+L)$
Lmct:	Calcareous schist lithic	
Lsa:	Argillite-shale lithic	
Lsac:	Calcareous argillite-shale lithic	
Lsc:	Sedimentary carbonate lithic	
Lsch:	Sedimentary chert or cherty argillite lithic	
Lsi	Sedimentary siltstone lithic	
M:	mica and chlorite flakes	
Op D:	Opaque dense minerals	
Nop D:	Nonopaque dense minerals	
Carb:	Carbonate minerals	
Zeol:	Zeolite grain(?) replacement	
Glau:	Glauconite	
Phsp:	Phosphatic debris	
Misc unid:	Other miscellaneous and unidentified grains	
Bio:	Siliceous and calcareous microfossils and bioclasts	
Inter cmt:	Interparticle cement (mainly carbonate)	
Total pts:	Total points counted	
Q = Qm + Qp	F = P + K + Fu + Palt	
L = Lm + Lv + Ls	Lv = Lvf + Lvv + Lvml + Lvl	
Lm = Lmv + Lmm + Lmt + Lma + Lmp + Lmct		
Ls = Lsa + Lsc + Lsch + Lsac + Lsi		

### Sites 977 and 978

Samples from Unit I at Site 977 and Unit I at Site 978 are compositionally similar with quartz as the most common monocrystalline component. Many of these quartz grains (individual grains and grains within quartz-mica tectonite lithic fragments) are inclusion rich and display undulatory extinction. Some polycrystalline quartz is present. Mica is common in both monocrystalline and polycrystalline (lithic) forms. Muscovite, biotite, and chlorite (included in mica category) are present, but muscovite is the most common. Biotite is typically altered to clay minerals. Lithic fragments are predominantly metamorphic: quartz-mica tectonite and locally polycrystalline-mica fragments are common (Pl. 2).

The only sample from Unit II at Site 977 that was examined in this study (Sample 161-977A-57X-CC, 33–34 cm) comes from a 1-cm-thick, granule-rich sand lamina recovered at the contact between Units I and II. The 40 cm of gravel recovered below this contact is comprised of volcanic and sedimentary rock fragments: common rhyodacite (phenocrysts of quartz, biotite, and plagioclase), limestone/dolomite, and quartz arenite, and minor andesite and basalt. The sand at the top of Unit II also consists predominantly of sedimentary and volcanic clasts with a lesser metamorphic component. Mineralogically mature sandstone/siltstone lithic fragments are common; they are composed of well-rounded to angular quartz grains, but locally contain trace amounts of feldspar grains, matrix, and carbonate cement. A range of other sedimentary lithic types is present including shale, foraminifer biocalcarenite, microsparite, cherty micrite, radiolarian chert, micrite, and foraminifer biomicrite (Pls. 2, 3). Volcanic clasts are rare to common in this sample and include rhyodacitic (phenocrysts of quartz, biotite, and plagioclase) and altered intermediate to mafic volcanic rocks with plagioclase microlites. A few clasts of granite (quartz + plagioclase + K-feldspar + biotite), quartz-mica tectonite (schist), and felsic tuff are present (Pl. 3). Using the Gazzi-Dickinson method, many of these lithic clasts are counted in

monomineralic categories because they contain sand-sized feldspar and quartz grains/crystals.

### Site 979

The main component of sand samples from Unit I at Site 979 is quartz (Table 2), both as individual grains and crystals within metamorphic lithic fragments. This quartz exhibits undulatory to straight extinction. Bioclastic debris is so abundant in Site 979 sand that it was counted only in a few samples and skipped in the remainder (Table 2). Other calcareous debris was counted as detrital sedimentary lithic fragments (Lsc) or coarse carbonate grains (Carb). Muscovite and biotite flakes are common, particularly biotite, which ranges from altered to pristine. Feldspar grains are typically fresh and consist predominantly of plagioclase, with lesser potassium feldspar. Glauconite is common in every sample, particularly as fecal pellets and foraminifer steinkerns (infillings). Metamorphic lithic fragments are mostly quartz-mica tectonite and polycrystalline mica. In addition to calcareous varieties, the sedimentary lithic fraction includes fragments of shale/argillite and siltstone. Volcanic lithic debris is for the most part concentrated in the uppermost (161-979A-2H-2, 96–97 cm) and lowermost (979A-55X-4, 140–142 cm and 58X-1, 80–82 cm) samples. It consists of fresh, altered, and devitrified colorless (felsic) to brown (intermediate to mafic) glassy fragments with predominantly vitric and lesser lathwork textures. Some felsitic volcanic lithic fragments are also present. The pristine glass fragments take a stain indicating both calcium- and potassium-rich varieties are present.

### Beach Sand

The beach samples collected along the southern Spanish coast generally consist of coarse, subangular to rounded, medium- to well-sorted sand. A similar range of grain types is found in all the samples, except one volcanoclastic sample (Table 2). Quartz is a major compo-

Table 2. Leg 161 and beach sand raw data and recalculated parameters.

Core, section, interval (cm)	Depth (mbsf)	Parameters																
		Qp	Qm	P	Palt zeol	F unst	K	Lvo	Lvf	Lvv	Lvml	Lvl	Lmv	Lmm	Lmt	Lma	Lmp	
161-974B-1H-3, 139-140	4.39	5	88	29	0	1	47	0	0	95	29	3	0	3	23	0	0	
2H-4, 63-65	11.63	1	110	42	0	12	72	0	3	6	4	0	0	7	50	13	8	
3H-4, 27-28	20.77	0	0	2	0	0	0	0	0	382	15	0	0	0	0	0	0	
4H-3, 12-13	28.62	0	95	58	0	3	63	0	3	3	0	0	0	11	53	14	9	
5H-3, 83-84	38.83	0	116	60	0	2	77	0	0	4	0	0	0	19	36	10	0	
6H-6, 132-133	53.32	0	104	33	0	0	53	0	0	0	1	0	0	29	88	28	12	
7H-3, 74-75	57.45	0	0	0	0	0	0	0	0	397	1	0	0	0	0	0	0	
9H-6, 116-118	81.56	0	0	19	0	0	16	0	2	292	57	4	0	0	1	1	3	
161-974B-22X-5, 56-57	200.66	4	128	12	0	0	19	0	0	0	0	0	0	3	15	0	0	
22X-6, 45-46	202.05	0	154	3	0	0	13	0	0	0	0	0	0	9	19	0	0	
22X-CC, 28-29	202.91	0	94	48	0	0	25	0	0	0	7	8	0	4	36	8	0	
161-976B-3H-1, 72-74	13.72	0	103	13	0	0	17	0	0	0	0	0	0	2	0	0	0	
6H-2, 85-87	43.85	0	111	16	0	0	9	0	0	0	0	0	0	0	0	0	0	
33X-2, 33-35	300.86	1	209	23	0	0	16	0	0	0	0	0	0	0	13	0	0	
161-976B-39X-CC, 24-26	364.89	6	176	8	0	0	12	0	0	0	0	0	20	3	67	0	0	
42X-CC, 15-16	386.75	0	138	12	0	0	6	0	0	0	0	0	0	5	55	0	0	
47X-CC, 10-14	440.24	0	83	3	0	0	4	0	0	0	0	0	0	7	11	27	0	
48X-1, 11-12	444.61	0	97	13	0	0	14	0	0	0	0	0	6	21	31	0	1	
51X-1, 45-4	473.8	0	101	3	0	0	4	0	0	1	0	0	0	18	61	0	4	
52X-1, 18-20	482.98	0	165	27	0	0	11	0	0	0	0	0	5	8	78	0	0	
58X-4, 117-119	539.63	0	169	19	0	0	28	0	0	0	0	0	1	8	85	0	0	
72X-2, 52-54	662.22	0	132	115	0	0	12	0	1	0	0	0	0	11	0	0	0	
72X-3, 91-93	663.89	0	69	109	105	0	4	0	2	2	13	8	0	0	5	0	0	
72X-CC, 16-18	664.23	0	88	113	0	0	70	0	0	13	12	15	0	1	13	0	0	
161-977A-22X-CC, 19-20	204.01	0	14	0	0	0	0	0	0	0	0	0	0	100	43	0	0	
27X-6, 129-130	251.39	0	103	0	0	0	0	0	0	0	0	0	0	26	38	0	0	
24X-4, 73-74	218.83	0	38	0	0	0	0	0	0	0	0	0	0	31	5	0	0	
25X-CC, 34-35	233.06	17	110	13	0	0	9	0	0	0	0	0	0	5	93	0	0	
27X-6, 29-130	251.39	0	103	0	0	0	0	0	0	0	0	0	0	28	38	0	0	
39X-1, 126-127	359.16	0	26	0	0	0	0	0	0	0	0	0	0	0	0	0	0	
52X-5, 76-77	489.66	0	254	0	0	0	20	0	0	0	0	0	0	0	39	0	0	
161-977A-57X-CC, 33-34	532.76	3	31	19	0	0	9	0	10	0	0	0	0	2	4	0	0	
161-979A-4R-1, 134-136	224.04	0	158	5	0	0	14	0	0	0	0	0	0	19	85	0	0	
6R-1, 70-72	236.9	0	162	5	0	0	13	0	0	0	0	0	0	20	89	0	0	
16R-2, 90-92	334.9	0	91	4	0	0	1	0	0	0	0	0	0	9	18	0	0	
161-979A-2H-2, 96-97	3.96	0	4	8	0	0	5	3	0	91	0	8	0	0	0	0	0	
9H-4, 76-78	73.26	0	176	14	0	0	8	0	0	0	0	0	1	2	27	0	0	
13H-CC, 22-24	116.43	2	176	18	0	0	4	0	0	0	0	0	5	1	30	0	0	
15H-3, 34-35	126.99	0	126	20	0	0	0	0	0	0	0	0	0	0	17	0	0	
24X-4, 125-126	211.45	2	136	12	0	0	4	0	0	0	0	0	0	0	35	0	0	
27X-3, 111-113	237.6	0	78	3	0	0	0	0	0	0	0	0	0	0	44	0	0	
33X-4, 8-10	295.96	0	188	8	0	0	6	0	0	0	0	0	0	0	12	0	0	
54X-3, 127-129	498.67	0	159	4	0	0	4	0	6	0	0	0	0	4	41	0	0	
55X-4, 140-142	509.8	0	222	12	0	0	3	0	3	56	0	0	1	0	14	0	0	
58X-1, 80-82	533.5	0	149	38	0	0	22	0	0	29	0	25	0	0	50	0	0	
Sample Beach location																		
1 = Beach at mouth of R. de Aguas (westernmost)		4	145	2	0	0	0	0	0	0	0	0	0	7	131	0	0	
2 = Beach 10 km east of Cabo de Gata		0	37	25	0	0	5	0	0	82	0	0	0	0	0	0	0	
3 = Beach at mouth of R. Andarax		0	59	0	0	0	0	0	0	0	0	0	0	0	119	0	0	
4 = Beach 5 km east of Castell de Ferro		0	48	9	0	0	0	0	0	0	0	0	0	9	125	0	0	
5 = Beach near mouth of R. Guadalfeo		0	50	4	0	0	0	0	0	0	0	0	0	2	107	0	0	
6 = Beach near mouth of R. Guadalhorce		6	150	20	0	0	1	0	0	0	0	0	33	1	82	0	0	
7 = Beach near mouth of R. Fuengirola		0	137	35	0	0	3	0	0	0	0	0	25	0	47	0	0	
8 = Beach near mouth of R. Guadalmanza		6	122	33	0	0	9	0	0	0	0	0	117	0	64	0	0	
9 = Beach 5 km east of Estepona		1	145	26	0	0	10	0	0	0	0	0	96	0	31	0	0	
10 = Beach east of Gibraltar (easternmost)		8	258	10	0	0	2	0	0	0	0	0	21	1	63	0	0	

Note: See Table 1 for definition of abbreviations; avg. = mean; std = standard deviation, asterisk in column indicates bioclasts not counted.

Table 2 (continued).

Core, section, interval (cm)	Depth (mbsf)	Lmct	Lsa	Lsac	Lsc	Lsch	Lsi	M	Op		Carb	Zeol	Glau	Phsp	Misc und	Carb bio	Inter cmt	Total pts
									D	Op D								
161-974B-1H-3, 139-140	4.39	0	7	4	2	1	0	11	0	8	30	1	7	3	3	*	3	403
2H-4, 63-65	11.63	0	20	8	2	4	0	26	0	3	3	0	0	0	6	*	0	400
3H-4, 27-28	20.77	0	0	0	0	0	0	0	0	0	0	0	0	0	1	*	0	400
4H-3, 12-13	28.62	0	0	0	0	0	0	68	1	7	10	0	0	0	2	*	0	400
5H-3, 83-84	38.83	0	0	0	0	0	0	70	0	0	5	0	1	0	0	*	0	400
6H-6, 132-133	53.32	0	1	0	0	0	0	32	0	8	11	0	0	0	0	*	0	400
7H-3, 74-75	57.45	0	0	0	0	0	0	1	0	0	0	0	0	0	1	*	0	400
9H-6, 116-118	81.56	0	1	0	0	1	0	1	0	1	1	0	0	0	0	*	0	400
161-974B-22X-5, 56-57	200.66	0	94	4	2	0	0	48	0	0	64	0	4	0	3	*	0	400
22X-6, 45-46	202.05	0	75	2	72	0	0	27	0	0	22	0	2	0	2	*	0	400
22X-CC, 28-29	202.91	0	1	0	11	0	0	8	0	3	2	0	0	0	0	*	0	253
161-976B-3H-1, 72-74	13.72	0	11	0	0	0	0	3	0	0	3	0	0	0	0	24	0	176
6H-2, 85-87	43.85	0	3	0	0	0	0	11	0	0	1	0	0	0	0	45	0	196
33X-2, 33-35	300.86	0	4	0	4	0	0	14	0	0	9	0	0	0	0	62	0	355
161-976B-39X-CC, 24-26	364.89	0	0	0	29	0	0	0	3	1	62	0	0	0	0	13	0	400
42X-CC, 15-16	386.75	0	0	0	16	0	0	30	5	0	79	0	0	0	6	26	0	378
47X-CC, 10-14	440.24	0	10	7	0	0	0	3	2	2	47	0	0	0	23	14	112	372
48X-1, 11-12	444.61	0	0	0	32	0	0	19	1	0	50	0	0	0	1	9	105	400
51X-1, 45-4	473.8	0	0	0	21	0	0	14	1	0	60	0	0	0	5	17	90	400
52X-1, 18-20	482.98	0	0	0	6	0	0	0	4	0	90	6	0	0	0	*	0	400
58X-4, 117-119	539.63	0	0	0	38	0	0	17	0	0	42	0	0	0	0	13	0	400
72X-2, 52-54	662.22	1	0	0	1	0	0	28	1	0	28	59	5	0	0	6	0	400
72X-3, 91-93	663.89	0	0	0	6	0	0	28	0	0	7	41	1	0	0	0	0	400
72X-CC, 16-18	664.23	0	8	1	2	0	0	37	0	0	25	1	2	0	0	1	0	400
161-977A-22X-CC, 19-20	204.01	0	0	0	0	0	0	85	10	23	0	0	0	0	0	*	0	275
27X-6, 129-130	251.39	0	0	0	0	0	0	37	0	0	5	0	0	0	0	*	0	209
24X-4, 73-74	218.83	0	0	0	0	0	0	30	0	0	0	0	0	0	0	*	0	104
25X-CC, 34-35	233.06	0	30	0	55	0	3	14	1	0	12	0	38	0	0	*	0	400
27X-6, 29-130	251.39	0	0	0	0	0	0	37	0	0	5	0	0	0	0	*	0	209
39X-1, 126-127	359.16	0	0	0	0	0	0	1	0	0	25	0	0	0	0	348	0	400
52X-5, 76-77	489.66	0	5	0	0	1	0	3	0	0	70	0	2	0	0	*	0	394
161-977A-57X-CC, 33-34	532.76	0	1	0	4	0	9	0	2	0	0	0	0	0	0	*	0	94
161-979A-4R-1, 134-136	224.04	0	0	0	34	0	0	27	11	0	47	0	0	0	0	*	0	400
6R-1, 70-72	236.9	0	0	0	41	0	0	24	4	0	49	0	0	0	0	*	0	407
16R-2, 90-92	334.9	0	0	0	2	0	0	16	18	0	9	0	0	0	0	*	0	168
161-979A-2H-2, 96-97	3.96	0	0	0	0	0	0	0	0	0	0	0	20	0	23	202	0	364
9H-4, 76-78	73.26	0	38	0	6	0	0	42	24	0	20	0	46	0	0	*	0	400
13H-CC, 22-24	116.43	0	15	0	12	0	0	17	6	0	37	0	77	0	0	*	0	400
15H-3, 34-35	126.99	0	0	0	2	0	0	10	3	0	49	0	48	0	0	125	0	400
24X-4, 125-126	211.45	0	114	0	43	0	17	5	3	3	7	0	19	0	0	*	0	400
27X-3, 111-113	237.6	0	150	0	36	0	0	2	0	0	5	0	82	0	0	*	0	400
33X-4, 8-10	295.96	0	38	0	14	0	0	24	0	1	20	0	82	0	7	*	0	400
54X-3, 127-129	498.67	0	33	0	65	0	0	12	0	0	34	0	38	0	0	*	0	400
55X-4, 140-142	509.8	0	0	0	4	0	0	12	6	0	26	0	39	0	2	*	0	400
58X-1, 80-82	533.5	0	0	0	0	0	0	5	3	0	44	0	35	0	0	*	0	400
Sample Beach location																		
1 = Beach at mouth of R. de Aguas (westernmost)		0	6	0	17	0	0	6	18	0	3	0	0	0	0	*	0	339
2 = Beach 10 km east of Cabo de Gata		0	0	0	0	0	0	2	0	0	0	34	0	0	0	*	0	185
3 = Beach at mouth of R. Andarax		0	0	0	33	0	0	0	28	4	6	0	0	0	0	*	0	249
4 = Beach 5 km east of Castell de Ferro		0	0	0	0	0	0	0	9	0	2	18	0	0	0	*	0	218
5 = Beach near mouth of R. Guadalfeo		0	0	0	0	0	0	0	14	0	0	0	0	0	0	*	0	177
6 = Beach near mouth of R. Guadalhorce		0	25	0	29	0	4	0	0	0	0	0	0	0	0	*	0	351
7 = Beach near mouth of R. Fuengirola		0	0	0	8	0	0	0	3	0	0	0	0	0	0	*	0	258
8 = Beach near mouth of R. Guadalmana		0	0	0	9	0	0	0	0	0	0	0	0	0	0	*	0	360
9 = Beach 5 km east of Estepona		0	17	0	2	0	0	0	0	0	0	0	0	0	0	*	0	328
10 = Beach east of Gibraltar (easternmost)		0	0	0	7	0	0	4	0	1	4	0	0	0	3	*	0	400

Table 2 (continued).

Core, section, interval (cm)	Depth (mbsf)	QFL%			QmFLt%			LmLvLs%			QmKP%			
		Q	F	L	Qm	F	Lt	Lm	Lv	Ls	Qm	K	P	
161-974B-1H-3, 139-140	4.39	27.6	22.8	49.6	26.1	22.8	51.0	15.6	76.0	8.4	53.3	28.5	18.2	
2H-4, 63-65	11.63	30.7	34.8	34.5	30.4	34.8	34.8	62.4	10.4	27.2	46.6	30.5	22.9	
3H-4, 27-28	20.77	0.0	0.5	99.5	0.0	0.5	99.5	0.0	100.0	0.0	0.0	0.0	100.0	
4H-3, 12-13	28.62	30.4	39.7	29.8	30.4	39.7	29.8	93.5	6.5	0.0	43.4	28.8	27.9	
5H-3, 83-84	38.83	35.8	42.9	21.3	35.8	42.9	21.3	94.2	5.8	0.0	45.5	30.2	24.3	
6H-6, 132-133	53.32	29.8	24.6	45.6	29.8	24.6	45.6	98.7	0.6	0.6	54.7	27.9	17.4	
7H-3, 74-75	57.45	0.0	0.0	100.0	0.0	0.0	100.0	0.0	100.0	0.0				
9H-6, 116-118	81.56	0.0	8.8	91.2	0.0	8.8	91.2	1.4	98.1	0.6	0.0	45.7	54.3	
		Avg	19.3	21.8	58.9	19.1	21.8	59.2	45.7	49.7	4.6	34.8	27.4	37.9
		Std	16.1	17.1	32.7	16.0	17.1	32.5	45.9	47.6	9.6	24.1	13.6	30.1
161-974B-22X-5, 56-57	200.66	47.0	11.0	42.0	45.6	11.0	43.4	15.3	0.0	84.7	80.5	11.9	7.5	
22X-6, 45-46	202.05	44.4	4.6	51.0	44.4	4.6	51.0	15.8	0.0	84.2	90.6	7.6	1.8	
22X-CC, 28-29	202.91	38.8	30.2	31.0	38.8	30.2	31.0	64.0	20.0	16.0	56.3	15.0	28.7	
		Avg	43.4	15.3	41.3	42.9	15.3	41.8	31.7	6.7	61.6	75.8	11.5	12.7
		Std	4.2	13.3	10.0	3.6	13.3	10.1	28.0	11.5	39.5	17.6	3.7	14.2
161-976B-3H-1, 72-74	13.72	70.5	20.5	8.9	70.5	20.5	8.9	15.4	0.0	84.6	77.4	12.8	9.8	
6H-2, 85-87	43.85	79.9	18.0	2.2	79.9	18.0	2.2	0.0	0.0	100.0	81.6	6.6	11.8	
33X-2, 33-35	300.86	77.8	14.4	7.8	77.4	14.4	8.1	61.9	0.0	38.1	84.3	6.5	9.3	
		Avg	76.1	17.6	6.3	75.9	17.6	6.4	25.8	0.0	74.2	81.1	8.6	10.3
		Std	4.9	3.1	3.6	4.9	3.1	3.7	32.2	0.0	32.2	3.5	3.6	1.3
161-976B-39X-CC, 24-26	364.89	56.7	6.2	37.1	54.8	6.2	38.9	75.6	0.0	24.4	89.8	6.1	4.1	
42X-CC, 15-16	386.75	59.5	7.8	32.8	59.5	7.8	32.8	78.9	0.0	21.1	88.5	3.8	7.7	
47X-CC, 10-14	440.24	49.1	4.1	46.7	49.1	4.1	46.7	78.5	0.0	21.5	92.2	4.4	3.3	
48X-1, 11-12	444.61	45.1	12.6	42.3	45.1	12.6	42.3	64.8	0.0	35.2	78.2	11.3	10.5	
51X-1, 45-4	473.8	47.4	3.3	49.3	47.4	3.3	49.3	79.0	1.0	20.0	93.5	3.7	2.8	
52X-1, 18-20	482.98	55.0	12.7	32.3	55.0	12.7	32.3	93.8	0.0	6.2	81.3	5.4	13.3	
58X-4, 117-119	539.63	51.5	14.3	34.1	51.5	14.3	34.1	66.1	0.0	33.9	78.2	13.0	8.8	
		Avg	52.0	8.7	39.2	51.8	8.7	39.5	76.7	0.1	23.2	86.0	6.8	7.2
		Std	5.2	4.5	6.9	5.0	4.5	6.9	9.7	0.4	9.7	6.6	3.8	4.0
72X-2, 52-54	662.22	48.4	46.5	5.1	48.4	46.5	5.1	85.7	7.1	7.1	51.0	4.6	44.4	
72X-3, 91-93	663.89	21.4	67.5	11.1	21.4	67.5	11.1	13.9	69.4	16.7	24.0	1.4	74.6	
72X-CC, 16-18	664.23	26.3	54.8	18.9	26.3	54.8	18.9	22.2	63.5	14.3	32.5	25.8	41.7	
		Avg	32.0	56.3	11.7	32.0	56.3	11.7	40.6	46.7	12.7	35.8	10.6	53.6
		Std	14.4	10.6	6.9	14.4	10.6	6.9	39.3	34.4	5.0	13.8	13.3	18.3
161-977A-22X-CC, 19-20	204.01	8.9	0.0	91.1	8.9	0.0	91.1	100.0	0.0	0.0	100.0	0.0	0.0	
27X-6, 129-130	251.39	61.7	0.0	38.3	61.7	0.0	38.3	100.0	0.0	0.0	100.0	0.0	0.0	
24X-4, 73-74	218.83	51.4	0.0	48.6	51.4	0.0	48.6	100.0	0.0	0.0	100.0	0.0	0.0	
25X-CC, 34-35	233.06	37.9	6.6	55.5	32.8	6.6	60.6	52.7	0.0	47.3	83.3	6.8	9.8	
27X-6, 29-130	251.39	61.7	0.0	38.3	61.7	0.0	38.3	100.0	0.0	0.0	100.0	0.0	0.0	
39X-1, 126-127	359.16	100.0	0.0	0.0	100.0	0.0	0.0				100.0	0.0	0.0	
52X-5, 76-77	489.66	79.6	6.3	14.1	79.6	6.3	14.1	86.7	0.0	13.3	92.7	7.3	0.0	
		Avg	57.3	1.8	40.8	56.6	1.8	41.6	89.9	0.0	10.1	96.6	2.0	1.4
		Std	29.2	3.1	29.4	29.8	3.1	29.9	19.0	0.0	19.0	6.5	3.4	3.7
161-977A-57X-CC, 33-34	532.76	37.0	30.4	32.6	33.7	30.4	35.9	20.0	33.3	46.7	52.5	15.3	32.2	
161-979A-4R-1, 134-136	224.04	50.2	6.0	43.8	50.2	6.0	43.8	75.4	0.0	24.6	89.3	7.9	2.8	
6R-1, 70-72	236.9	49.1	5.5	45.5	49.1	5.5	45.5	72.7	0.0	27.3	90.0	7.2	2.8	
16R-2, 90-92	334.9	72.8	4.0	23.2	72.8	4.0	23.2	93.1	0.0	8.9	94.8	1.0	4.2	
		Avg	57.4	5.2	37.5	57.4	5.2	37.5	80.4	0.0	19.6	91.4	5.4	3.3
		Std	13.4	1.0	12.4	13.4	1.0	12.4	11.1	0.0	11.1	3.0	3.8	0.8
161-979A-2H-2, 96-97	3.96	3.4	10.9	85.7	3.4	10.9	85.7	0.0	100.0	0.0	23.5	29.4	47.1	
9H-4, 76-78	73.26	65.7	7.5	26.9	65.7	7.5	26.9	41.7	0.0	58.3	89.8	3.1	7.1	
13H-CC, 22-24	116.43	67.7	8.4	24.0	66.9	8.4	24.7	57.1	0.0	42.9	88.9	2.0	9.1	
15H-3, 34-35	126.99	76.4	12.1	11.5	76.4	12.1	11.5	89.5	0.0	10.5	86.3	0.0	13.7	
24X-4, 125-126	211.45	38.0	4.4	57.6	37.5	4.4	58.1	16.7	0.0	83.3	89.5	2.8	7.9	
27X-3, 111-113	237.6	25.1	1.0	74.0	25.1	1.0	74.0	19.1	0.0	80.9	96.3	0.0	3.7	
33X-4, 8-10	295.96	70.7	5.3	24.1	70.7	5.3	24.1	18.8	0.0	81.3	93.1	3.0	4.0	
54X-3, 127-129	498.67	50.3	2.5	47.2	50.3	2.5	47.2	30.2	4.0	85.8	95.2	2.4	2.4	
55X-4, 140-142	509.8	70.5	4.8	24.8	70.5	4.8	24.8	19.2	75.6	5.1	93.7	1.3	5.1	
58X-1, 80-82	533.5	47.6	19.2	33.2	47.6	19.2	33.2	48.1	51.9	0.0	71.3	10.5	18.2	
		Avg	51.5	7.6	40.9	51.4	7.6	41.0	34.0	23.2	42.8	82.8	5.4	11.8
		Std	23.6	5.4	24.4	23.6	5.4	24.4	25.8	38.1	35.7	22.0	8.9	13.3
Sample Beach location														
1 = Beach at mouth of R. de Aguas (westernmost)		47.8	0.8	51.8	46.5	0.6	52.9	85.7	0.0	14.3	98.8	0.0	1.4	
2 = Beach 10 km east of Cabo de Gata		24.8	20.1	55.0	24.8	20.1	55.0	0.0	100.0	0.0	55.2	7.5	37.3	
3 = Beach at mouth of R. Andarax		28.0	0.0	72.0	28.0	0.0	72.0	78.3	0.0	21.7	100.0	0.0	0.0	
4 = Beach 5 km east of Castell de Ferro		25.1	4.7	70.2	25.1	4.7	70.2	100.0	0.0	0.0	94.2	0.0	15.8	
5 = Beach near mouth of R. Guadalfeo		30.7	2.5	86.9	30.7	2.5	86.9	100.0	0.0	0.0	92.6	0.0	7.4	
6 = Beach near mouth of R. Guadalhorce		44.4	6.0	49.6	42.7	6.0	51.3	66.7	0.0	33.3	87.7	0.6	11.7	
7 = Beach near mouth of R. Fuengirola		54.2	15.0	30.8	54.2	15.0	30.8	92.3	0.0	7.7	78.3	1.7	20.0	
8 = Beach near mouth of R. Guadalmanza		35.6	11.7	52.8	33.9	11.7	54.4	95.3	0.0	4.7	74.4	5.5	20.1	
9 = Beach 5 km east of Estepona		44.5	11.0	44.5	44.2	11.0	44.8	87.0	0.0	13.0	80.1	5.5	14.4	
10 = Beach east of Gibraltar (easternmost)		68.0	3.1	28.9	66.0	3.1	30.9	93.8	0.0	8.3	95.5	0.7	3.7	
		Avg	40.3	7.5	52.2	39.5	7.5	52.9	79.9	10.0	10.1	84.7	2.2	13.2
		Std	14.1	6.7	14.9	13.6	6.7	14.6	29.9	31.6	10.8	13.6	2.9	11.2

ment both as individual grains and crystals within metamorphic lithic fragments. Grains of plagioclase are common, whereas polycrystalline quartz, potassium feldspar, coarse carbonate, zeolite, biotite, and muscovite are minor constituents. Lithic fragments are predominantly metamorphic (Pl. 3), with common quartz-mica tectonite, serpentinite, and lesser quantities of polycrystalline mica. Locally, carbonate and argillite are the most common sedimentary lithic fragments (Pl. 3). Volcanic lithic fragments are limited to Sample #2 (see Table 2 for sample location) and consist of roughly equal proportions of orange/brown, altered and potassium-rich (yellow stained) colorless glass.

## SAND DETRITAL MODES

### Site 974

Detrital modes were determined for 11 samples from Site 974 (Table 2): eight from Unit I (Pleistocene) and three from Unit III (late Miocene). The Unit I samples are subdivided into resedimented ash and sand end-members. As shown in Figure 6, the Unit I sand has intermediate QFL and QmKP proportions, and for the most part, the lithic fraction is dominated by metamorphic components. In contrast, the Unit I resedimented ash samples are dominantly composed of volcanoclastic lithic fragments. One of the Unit III samples is similar in composition to the Unit I sand. The other two Unit III sand samples are quartzolithic with minor feldspar and a dominantly sedimentary lithic component.

### Site 976

Detrital modes were determined for 13 samples from Site 976: three from Unit I (Pleistocene), six from Unit II (Pliocene to Pleistocene), one from Unit III (lower Pliocene), and three from Unit IV (upper Miocene). As displayed in Figures 7–9, these samples form three compositional groups. Sand within Unit I is quartzose with a minor sedimentary lithic component. Unit II and III sand samples are quartzolithic with a dominantly metamorphic and lesser sedimentary lithic component. The Unit IV samples are feldspathic and characterized by a high proportion of plagioclase feldspar and volcanic-lithic components.

### Sites 977 and 978

Detrital modes were determined for eight samples from Site 977 and three from Site 978: seven from Unit I (Pleistocene–Pliocene) at Site 977, three from Unit I (Pliocene) at Site 978, and one from Unit II (lower Pliocene to Miocene?) at Site 977. Unit I sand samples from both sites show a range in composition that is essentially a function of variation between the proportions of quartz and metamorphic lithic components (Figs. 7–9). The one sample from Unit II contains subequal proportions of quartz, feldspar, and lithic fragments with a moderately high amount of potassium feldspar and metamorphic and sedimentary lithic fragments (Figs. 7–9).

### Site 979

Detrital modes were determined for 10 samples from Unit I (Pleistocene–upper Pliocene) at Site 979. Most samples show a range in composition that is essentially a function of variation between the proportions of quartz and lithic components (Figs. 7, 8). In terms of their lithic proportions, the samples fall into two groups: one that is relatively enriched in volcanic lithic fragments and a second dominated by sedimentary and metamorphic lithic fragments (Fig. 10).

## Beach Sand

Detrital modes were determined for 10 sand samples from modern beaches along the Spanish coast. These show a range in composition that is essentially a function of variation between the proportions of quartz, metamorphic lithic fragments, and, to a lesser degree, plagioclase feldspar content (Figs. 7, 8, 10). The lithic fraction of one sample is entirely volcanoclastic.

## SAND PROVENANCE

### Site 974

The Pleistocene volcanoclastic samples from Site 974 are essentially resedimented pyroclastic deposits composed almost entirely of volcanic glass (Comas, Zahn, Klaus, et al., 1996). These ashes are likely the product of individual felsic to intermediate eruptions in that the vitric components are colorless and are homogeneously stained (either red [Ca] or yellow [K]) throughout any given sample. There are three main Pleistocene volcanic provinces in the Tyrrhenian Sea: (1) high-potassic alkaline volcanics of mainland Italy to the east and northeast of Site 974 (Roman and Campanian volcanic areas); (2) isolated alkali-olivine and tholeiitic volcanic centers distributed from northern Sardinia across the axis of the Tyrrhenian Basin to eastern Sicily; and (3) to the southeast, within the Eolian magmatic arc, a calc-alkaline and shoshonitic magmatic province (Savelli, 1988). Given their proximity to Site 974, the first two provinces are the most likely sources of sand-sized ash at this site; however, detailed tephra studies (e.g., McCoy and Cornell, 1990) are needed to better constrain ash provenance through their chemical fingerprints.

The other non-ash sand samples from Unit I contain moderate amounts of plagioclase and potassium feldspar and all but one contain a high percentage of metamorphic lithic fragments; this composition suggests a continental source terrane. Site 974 lies in a north-south-oriented bathymetric low that is defined by basement uplifts and projects toward the northwest-southeast-oriented continental margin of Italy. Carter et al. (1972) and Vanney and Gennesseaux (1985) show a complex series of north-south-oriented submarine channels in the vicinity of Site 974 that extend and head toward the Italian continental shelf near the Tiber River delta. These channel orientations suggest that the Tiber River, or at least that coastal area, may have been a primary source of sediment at Site 974 during the Pleistocene. Outcrops in the Tiber River drainage basin include Pliocene–Pleistocene alkaline-potassic lava flows and pyroclastic rocks, and deformed (and metamorphosed?) Alpine turbidite and pelagic sequences (Bellotti et al., 1986; 1995). Seismic stratigraphy, and paleontological, sedimentological, and geochemical studies suggest that Unit III is a lacustrine (“Lago Mare”), synrift sequence (see Comas, Zahn, Klaus et al. [1996, p. 64] for discussion and additional references). Therefore, it is probable that local basement highs supplied clastic material to the Site 974 area during the Miocene. In fact, dredge hauls along the Monte de Marche, an uptilted basement block just south of Site 974, have yielded a Paleozoic to Neogene suite of phyllite, limestone, and granite fragments (Sartori et al., 1987) that is similar to the suite of lithic fragments present in sand from Unit III at Site 974, as described in this study, and at nearby Site 652, described by Borsetti et al. (1990). According to Selli (1985), these basement rocks are likely part of the Alpine suture zone.

### Alboran Sea

#### Beach Sand

Beach sand samples, particularly those near the mouths of major streams and rivers, were collected to provide information on the com-

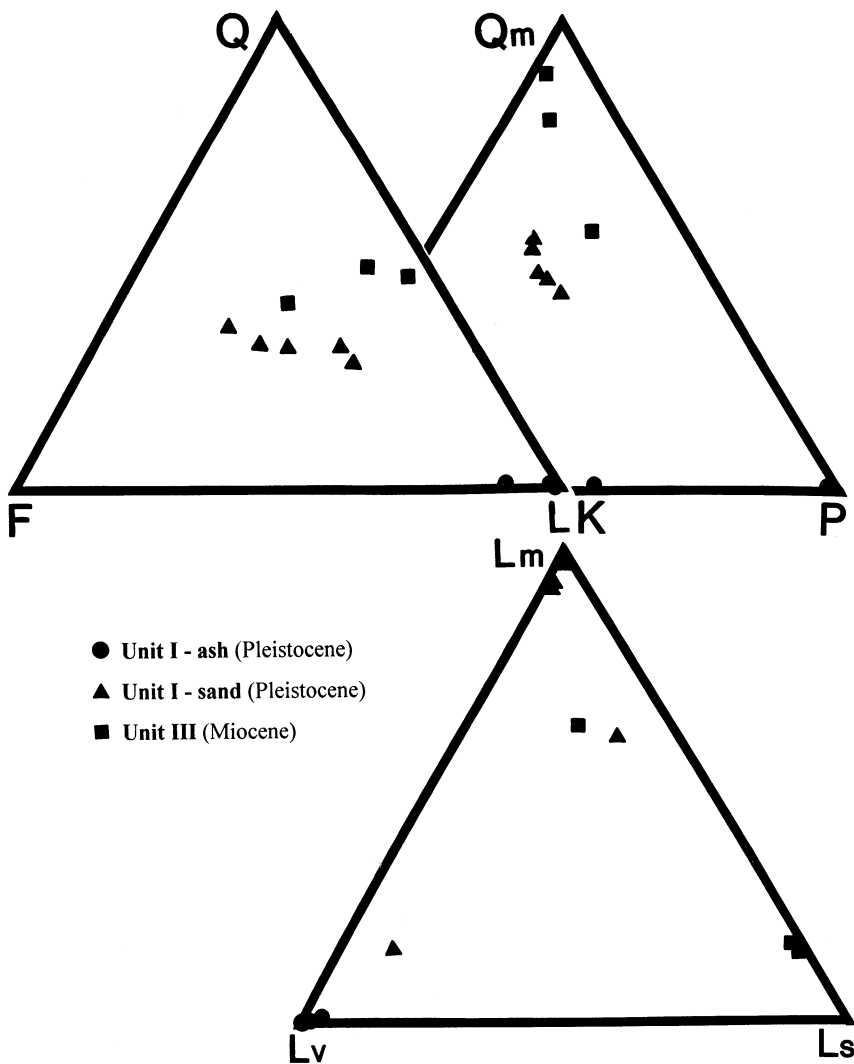


Figure 6. QFL, QmKP, and LmLvLs ternary plots for Site 974 sand samples where Q is total monocrystalline and polycrystalline quartz; F is total feldspar; L is total lithic fragments including extrabasinal carbonate lithic fragments; Qm is total monocrystalline quartz; K is total potassium feldspar; P is total potassium feldspar; Lm is total metamorphic lithic fragments including quartz-mica tectonite, polycrystalline mica, phyllite, and slate; Lv is total volcanic lithic fragments including vitric, microplitic, lathwork, and felsitic textures; and Ls is total sedimentary lithic fragments including argillite/shale, siltstone, sedimentary chert, and extrabasinal carbonate (limestone/dolomite).

positional characteristics of sand derived from modern Spanish coast terranes that likely served as sources for sand deposited at Sites 976, 978, and 979. These onshore source terranes (Fig. 5) include sedimentary Flysch Trough Units, rocks of the Alboran Domain (metamorphic and nonmetamorphic rocks of the Betic Cordillera), and volcanic rocks (onshore equivalents of the submarine ridges and seamounts that characterize the basin center; Comas et al., 1992). Outcrops of the sedimentary Flysch Trough Units are limited and represented by only the easternmost beach sample taken near Gibraltar (Sample #10; see Table 2 for sample location). This sample has the highest QFL%Q (68%; Table 2) of all the beach sands analyzed, and is thus the most compositionally mature, which could be attributed to the effects of sedimentary recycling. The Alboran Domain, the most extensive terrane that crops out along the coastal region (Fig. 5), contains high-pressure/low-temperature, low-pressure/high-temperature, and low-grade metamorphic rocks, including the Ronda peridotite massif (e.g., Chalouan and Michard, 1990; Goffé et al., 1989). As expected, the series of samples collected from beaches near the mouths of major streams and rivers that cross-cut Alboran Domain rocks are generally quartzolithic and metamorphiclastic with minor plagioclase and sedimentary lithic components. Serpentine fragments within these samples were likely derived from the Ronda peridotite

and are limited to samples collected between Malaga and Gibraltar (Fig. 5).

The diverse suite of volcanic rocks within the Alboran basin (e.g., calc-alkaline volcanic rocks [7–13 Ma], lamproites and shoshonitic lavas [4.5–9 Ma] and alkali basalts [1.5–6 Ma]; Bellon et al., 1983; Comas et al., 1992; Hernandez et al., 1987) is represented by only one beach sample taken from east of Almería (Sample #2; Table 2). This sample is composed entirely of volcanic lithic fragments, phenocrysts, and zeolite alteration minerals. It is noteworthy that in contrast to this sample, the other nine beach samples are completely devoid of volcanic lithic fragments.

#### Site 976

The Site 976 data cluster into three discrete petrographic groups that are stratigraphically distinct. The provenance of each group, from oldest to youngest, is discussed below.

Given the relict pyroclastic textures (e.g., pumice), high plagioclase phenocryst(?) content, presence of embayed biotite phenocrysts, and high percentage of zeolite alteration minerals, Unit IV likely had a significant volcanic component before undergoing burial diagenesis. The uniform composition/alteration of the vitric frag-

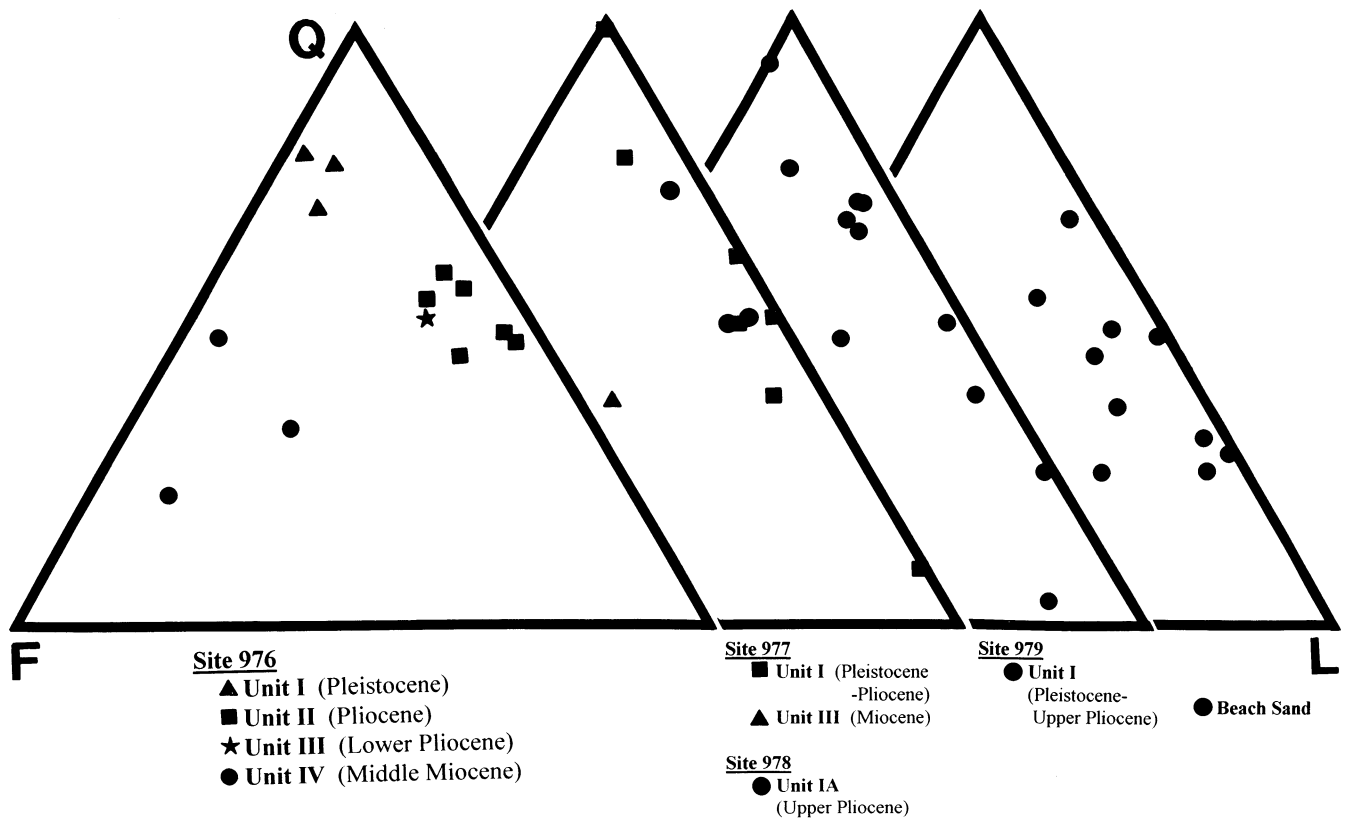


Figure 7. QFL ternary plots of Site 976–979 and beach sand samples where Q is total monocrySTALLINE and polycrystalline chert, F is total feldspar, and L is total lithic fragments including extrabasinal carbonate lithic fragments.

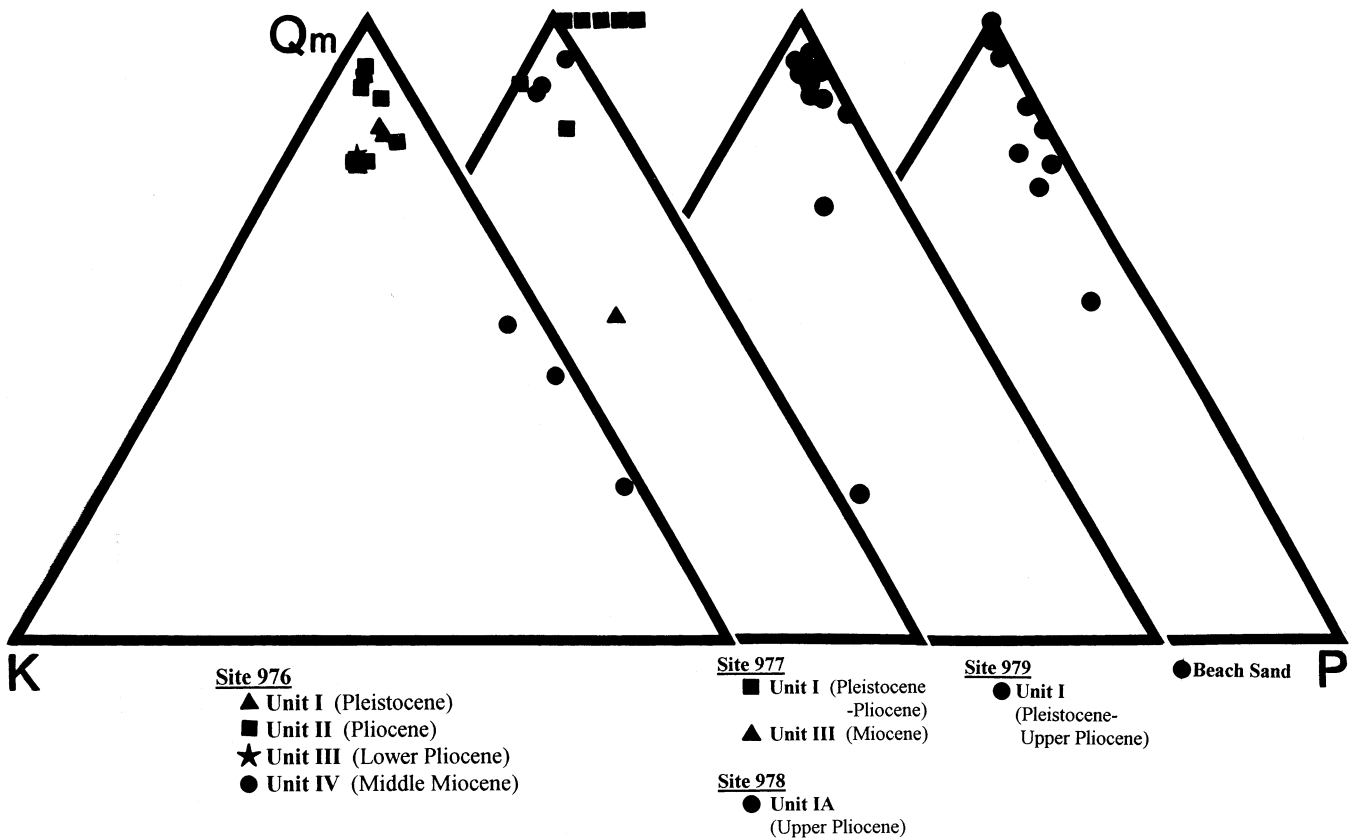


Figure 8. QmKP ternary plots of Site 976–979 and beach sand samples where Qm is total monocrySTALLINE quartz, K is total potassium feldspar, and P is total potassium feldspar.

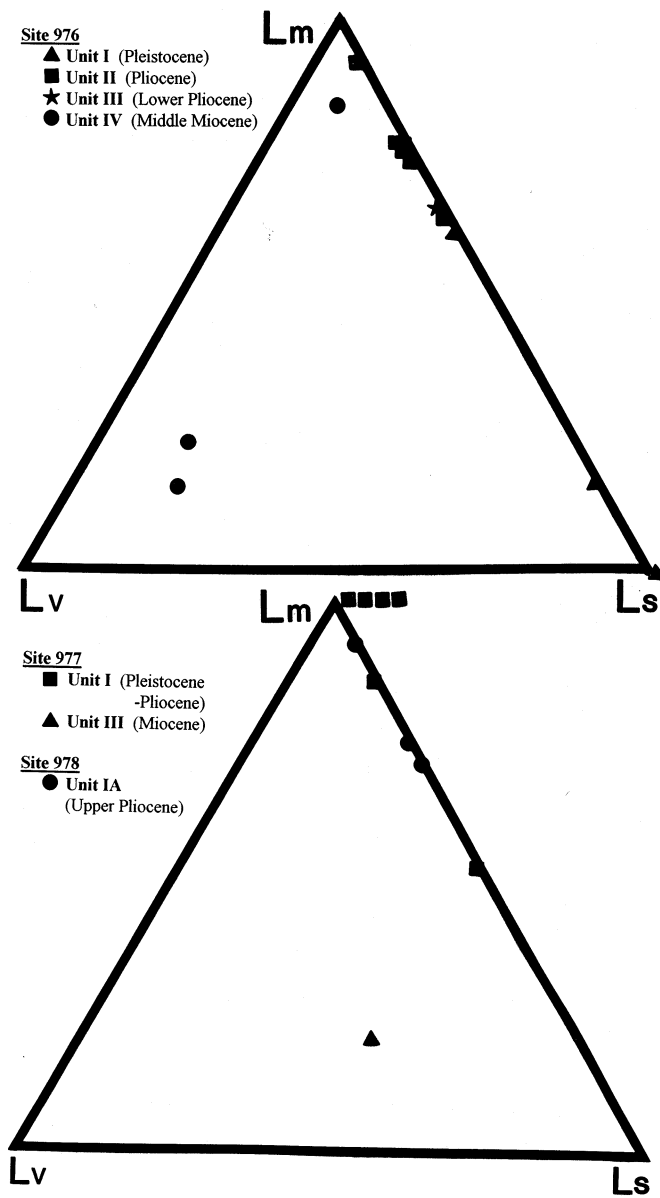


Figure 9. LmLvLs ternary plots of Site 976–978 sand samples where Lm is total metamorphic lithic fragments including quartz-mica tectonite, polycrystalline mica, phyllite, and slate; Lv is total volcanic lithic fragments including vitric, microlitic, lathwork, and felsitic textures; and Ls is total sedimentary lithic fragments including argillite/shale, siltstone, sedimentary chert, and extrabasinal carbonate (limestone/dolomite).

ments is consistent with a single eruptive source of pyroclastic material that was likely associated with a middle to upper Miocene pulse of calc-alkaline magmatism that has been documented across the Alboran Basin (Comas et al., 1992). Shipboard biostratigraphic analysis yielded a middle Miocene age (Serravallian: 13.5–10.5 Ma) for Unit IV, but radiometric age dating of biotite from Unit IV may further constrain timing of the source eruption. Unit IV contains interspersed pebbles to sand-sized metamorphic rock fragments similar to underlying basement lithologies at Site 976 (e.g., high-grade pelitic schist, pelitic paragneiss, marble, and calc-silicate rock; Comas, Zahn, Klaus, et al., 1996), as well as onshore outcrops of Alboran Domain rocks. This polymictic lithic assemblage, along with the presence of a mixed deep- and shallow-water fauna (Comas, Zahn, Klaus, et al., 1996), implies that Unit IV is not a primary pyroclastic deposit,

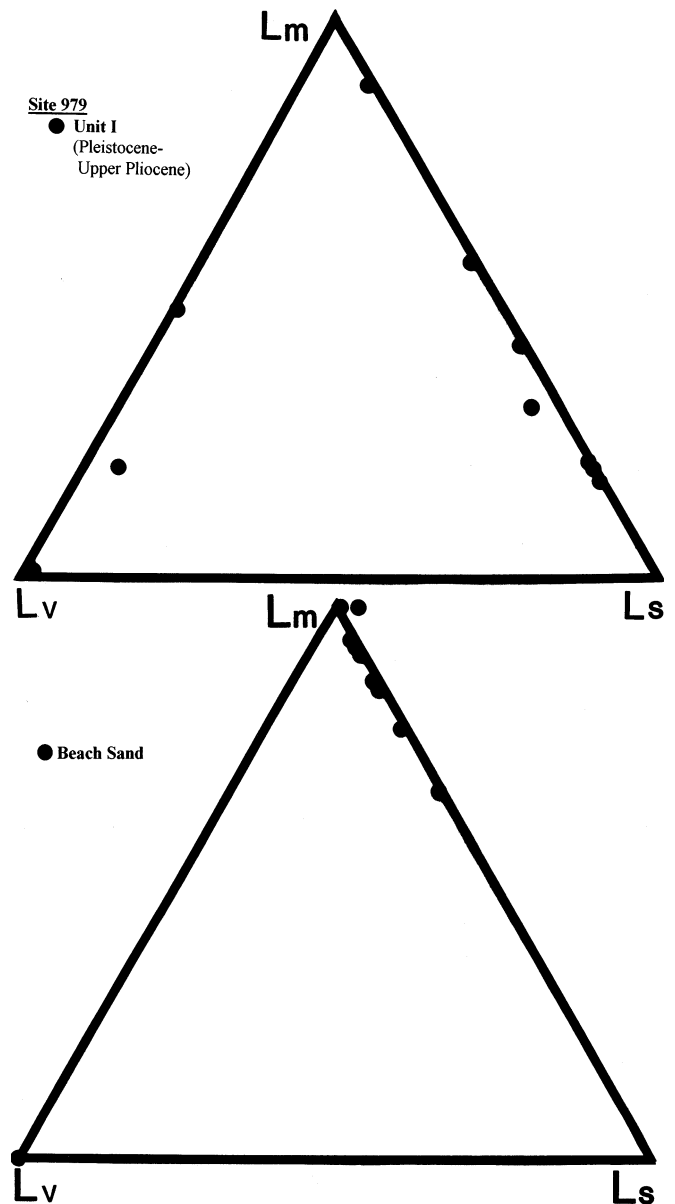


Figure 10. LmLvLs ternary plots of Site 979 and beach sand samples where Lm is total metamorphic lithic fragments including quartz-mica tectonite, polycrystalline mica, phyllite, and slate; Lv is total volcanic lithic fragments including vitric, microlitic, lathwork, and felsitic textures; and Ls is total sedimentary lithic fragments including argillite/shale, siltstone, sedimentary chert, and extrabasinal carbonate (limestone/dolomite).

but was likely redeposited and is therefore epiclastic. Alonso et al. (Chap. 4, this volume) propose that Unit IV consists of debris-flow deposits.

Because the thin sand layers in the upper part of Unit III (Fig. 3) are very similar in composition to those in Unit II, they likely had the same provenance and are likely part of the same depositional system. The source of the thick turbidite sequence of Units II/III was probably a submarine canyon that headed somewhere along the continental margin to the north; Alonso et al. (Chap. 4, this volume) favor the Fuengirola River as the major source of sediment at Site 976, based on the proximity of the Fuengirola Canyon to Site 976. Onshore beach sands contain components similar to those found in Units II and III at Site 976, but the beach sand is richer in lithic material, with a particularly high proportion of serpentinite fragments likely derived from

the Ronda peridotite (Pl. 3). Serpentine is a soft mineral, and it is possible that during increased fluvial transport associated with sea level lowstands, serpentinite fragments were more easily abraded and preferentially lost. Such a scenario would explain the lower content of serpentinite fragments in the Site 976 turbidite samples (maximum framework percent = 5%) as compared with onshore beach samples to the north (maximum framework percent = 10% in Samples #6 and #7; Table 2). If serpentinite (Lmv) is removed from the grain totals and the formulas used for recalculating parameters (Table 1), the mean composition of sand from Units II/III at Site 976 ( $Q_{53}F_0L_{38}$ ;  $Qm_{86}K_7P_7$ ;  $Lm_{75}Lv_0Ls_{25}$ ) is strikingly similar to the average composition of the two beach sand samples north of Site 976 (average of beach samples #7 and #6:  $Q_{55}F_{12}L_{34}$ ;  $Qm_{83}K_1P_{16}$ ;  $Lm_{74}Lv_0Ls_{26}$ ; Table 2). Feldspar ratios are less correlative, however, with the beach sand relatively depleted in potassium feldspar. This could be a function of a difference in transport history (fluvial/beach vs. fluvial/deltaic/turbidite) and/or climate, both of which are known to affect feldspar ratios (e.g., Kairo et al., 1993; Marsaglia et al., 1996; Sedimentology Seminar, 1988). Note that beach sand to the northwest of Site 976 is even more enriched in serpentinite fragments (maximum content of 33% of the framework grains in Sample #8; Table 2), making a north-western source less likely.

In contrast to the strong clastic pulse of Unit II, during the accumulation of Unit I sediments, Site 976 only received sporadic sand input. The composition of this sand is distinct from that found in the underlying units in that it is very quartzose and lithic poor, and resembles modern quartz-rich sands described by Huang and Stanley (1972) from shallow piston cores in the deeper part of the Western Alboran Basin. Huang and Stanley (1972) propose that the major source of the piston-cored sand is the Strait of Gibraltar area and adjacent Spanish slope, where coastal outcrops consist of sedimentary Flysch Trough Units (e.g., Aljibe quartz arenites with >98% quartz grains; Stromberg and Bluck, 1998) that would likely produce second-cycle, quartzose sand (Fig. 5). The more quartzose composition of beach sand from the Gibraltar area (68%; Sample #10; Table 2) supports this hypothesis. Therefore, we propose that the compositional shift from Unit II/III to Unit I sand likely results from a westward shift in source area. The strong east-flowing bottom currents needed to erode and transport this sediment from the Gibraltar area may have been generated by estuarine circulation during glacial minima when surface waters were freshened (Huang and Stanley, 1972). This scenario seems more plausible than that of the Shipboard Scientific Party (1973) who proposed that the quartzose sand in the correlative Quaternary section at DSDP Site 121 (Fig. 5) may have been deposited by melting icebergs carried into the Mediterranean from the Atlantic Ocean during glacial maxima.

#### Sites 977 and 978

The Almería channel is one of the major submarine canyons/channels in the Alboran Sea and the only channel that extends into the Eastern Alboran Basin (Alonso and Maldonado, 1992; Carter et al., 1972; Vanney and Genesseeux, 1985); as such, it likely provides the main conduit for terrigenous sediment carried into the Eastern Alboran Basin and Sites 977 and 978. This long, well-developed channel initiates in the coastal embayment between Almería and the Chella Bank, and extends southward feeding into the Alboran Channel, a major Pleistocene–Pliocene sediment depocenter that extends from the middle of the Alboran Basin eastward toward Sites 977 and 978 (Figs. 3, 5; Alonso and Maldonado, 1992). The main drainage of the Almería coastal embayment is the Andarax River, a seasonal ephemeral stream that empties into the Alboran Sea at Almería. Modern beach sand collected near the mouth of the Andarax River shows it to be predominantly composed of quartz-mica tectonite fragments, carbonate lithic fragments, and quartz (Pl. 3; Table 2).

Although detrital modes of sand samples from Unit I at Site 977 and Unit I at 978 are highly variable, they exhibit similar mean compositions. For example QFL%Q varies from 8% to 100% at Site 977, and from 49% to 73% at Site 978, but the mean QFL%Q for each is 57%. In contrast, beach sand from the mouth of the Andarax River has a relatively low QFL%Q of 28%. The metamorphic and sedimentary lithic populations within Site 977 and 978 sands are similar to those found in onshore beach sand samples, but the proportions of these components vary. This lack of direct correlation could be a product of one or more of the following: (1) the beach sampled is not representative of modern Andarax River sediment; (2) the composition of Andarax River sediment has changed through time, perhaps because of changes in drainage basin size; (3) there is an inherent dependence of composition on grain size in sand derived from Alboran Domain rocks, with lithic components enriched in coarser beach sand and quartz enriched in the finer grained turbidites at Site 977 and 978; and (4) metamorphic and sedimentary lithic fragments are preferentially abraded/removed during sand transport down the Almería Channel and through the Alboran Trough. Although the precise source of Unit I sand at Site 977 and 978 is equivocal, the lack of volcanoclastic debris effectively rules out derivation from onshore or offshore volcanic provinces and the submarine physiography strongly supports an Andarax River source via the Almería Channel.

In contrast, the single sand sample analyzed from Unit II at Site 977, as well as the underlying gravel described by shipboard scientists has a significant volcanic lithic component. As discussed in Comas et al. (1996), Unit II gravel not only contains rhyodacite pebbles similar to samples from the Al-Mansour Seamount, but also basalt and andesite pebbles similar to the volcanic rocks found to the west on the Alboran Ridge and to the north on Cabo de Gata. Thus Unit II sand and gravel may have been locally derived, or, alternatively, far-traveled.

#### Site 979

The physiography of the Southern Alboran Basin where Site 979 is located (Fig. 3) suggests that possible sand sources are limited to the North African coast between Melilla and Al-Hoseima and the submarine volcanic ridges that surround the basin (Fig. 4). The Unit I sand at Site 979 is generally quartzolitic, but with variable lithic proportions. Volcanic lithic fragments (glassy shards) are most abundant in the uppermost sample (<0.085 Ma) and the lowermost part of the section (Pliocene; > 2.63 Ma), below a possible hiatus at 476 mbsf (Comas, Zahn, Klaus, et al., 1996). Given that the basin is surrounded by volcanic terranes, the source(s) of this vitric component is equivocal. In addition, no discrete source canyon is present along the North African coast south of Site 979, where the coastal zone is characterized by a broad shallow (<100 m) shelf (Fig. 3). The high percentage of glauconite and bioclastic debris (the percentage of bioclastic debris was so high it was not tallied in most samples) in Site 979 samples is consistent with redistribution from the shallow shelf environment into the basin via turbidity currents. In contrast to the southern Spanish margin, outcrops along the North African coast, due south of Site 979, are dominantly sedimentary, with lesser volcanic and metamorphic rocks (Fig. 4); this change in source terrane is reflected in the relatively high sedimentary lithic proportions of many samples from Site 979 (Fig. 10). However, there is a crude tendency for the older (deeper) samples to contain more sedimentary lithic fragments and the younger samples to contain more metamorphic lithic fragments (Table 2).

#### Sand Detrital Modes and Tectonic Setting

Quantitative detrital modes of sandstones have been closely tied to the tectonic settings of their provenance terranes. Based on compi-

lations of detrital modes, Dickinson et al. (1983) outlined three main provenance fields on a QFL ternary diagram: Continental Block, Magmatic Arc, and Recycled Orogenic. Quartzose sandstones derived from subduction complexes or fold-thrust belts constitute the Recycled Orogenic provenance group, which Dickinson et al. (1983) further divide into Quartzose-, Transitional- and Lithic-Recycled subfields on a QmFLt ternary plot. Mean values for most of the subgroups outlined at the Alboran and Tyrrhenian Sea sites plot in the Recycled Orogenic field and near the boundary of the Quartzose- and Transitional-Recycled subfields (Fig. 11). Exceptions include Unit I Pleistocene sand at Site 974 and Unit IV Miocene sand at Site 976, which plot in Magmatic Arc fields, and the Unit I Pleistocene sand at Site 976, which plots near the join between Recycled Orogenic and Transitional Continental fields (Fig. 11). Note that the likely diagenetic alteration and dissolution of volcanic debris within Unit IV sand at Site 976 suggest that the sand's true mean composition should be shifted towards the lithic end of the Magmatic Arc field (arrow in Fig. 11), and that the composition of the lower Pliocene to Miocene sand from Unit II at Site 977 falls in the Dissected Arc field. Sand within the Alboran and Tyrrhenian Basins has a mixed metamorphic, volcanic, and sedimentary provenance reflecting the unique "Mediterranean-style" tectonic histories of these basins: collisional orogen followed by extension and related volcanism. Crude temporal trends, such as that from more volcanoclastic (Miocene) to metamorphoclastic (Pliocene–Pleistocene) compositions in the Alboran Basin, and from metamorphoclastic (Miocene) to volcanoclastic (Pleistocene) compositions in the Tyrrhenian Sea, can be linked to changes in tectonic regime, with the volcanoclastic intervals representing periods of active extension and volcanism. It is important to note that Pleistocene sand from Site 974 in the Tyrrhenian backarc basin ( $Q_{19}F_{22}L_{59}$ ;  $Lm_{46}Lv_{50}Ls_{5}$ ) is very similar in composition to Pleistocene sand from the Japan Sea continental-backarc basin (e.g., Site 299;  $Q_{13}F_{25}L_{62}$ ;  $Lm_{39}Lv_{38}Ls_{23}$ ; Marsaglia et al., 1992; Marsaglia and Ingersoll, 1992), although Site 974 is distinguished by a higher metamorphic lithic fraction. The latter could be considered as characteristic of sand deposited in backarc basins that develop in collisional settings.

Petrographic data from the Alboran and Tyrrhenian Seas form the basis of a preliminary actualistic model for interpreting sand provenance within remnant ocean basins caught up in complex suture zones. For example, the range of volcanoclastic, metamorphoclastic, and quartzose sand compositions that we find across these basins and within individual stratigraphic columns (e.g., Sites 976 and 974; Ta-

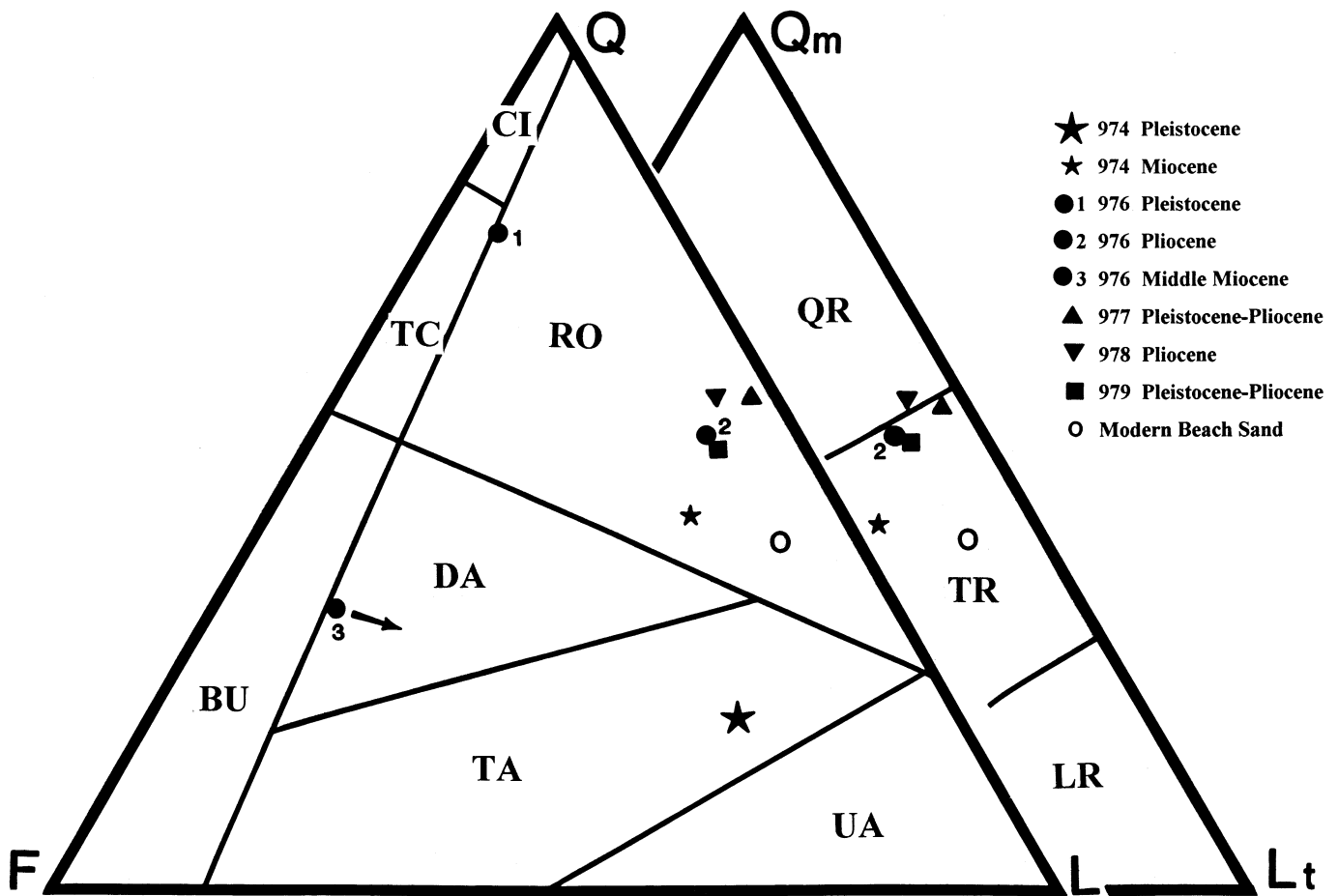


Figure 11. Mean sand compositions for Sites 974, 976, 977, 978 and 979, and beach samples (Table 2) plotted on QFL and QmFLt ternary diagrams where Q is total monocrystalline and polycrystalline chert; F is total feldspar; L is total lithic fragments including extrabasinal carbonate lithic fragments; Qm is total monocrystalline quartz; and Lt is total lithic fragments including extrabasinal carbonate lithic fragments plus polycrystalline quartz. Arrow indicates likely direction of compositional shift if altered volcanoclastic debris is underestimated in middle Miocene samples from Site 976. Compositional fields from Dickinson et al. (1983): CI = craton interior; TC = transitional continental; BU = basement uplift; RO = recycled orogenic; DA = dissected arc; TA = transitional arc; UA = undissected arc; QR = quartzose recycled; TR = transitional recycled; LR = lithic recycled.

ble 2) is strikingly similar to the suite of petrofacies documented by Critelli (1993) within the Liguride Complex, an accretionary wedge of the Southern Apennines. His Upper Cretaceous to middle Eocene quartzose petrofacies ( $Q_{90}F_9L_1$ ) corresponds to Unit I at Site 976 ( $Q_{76}F_{17}L_6$ ), his upper Oligocene volcanolithic petrofacies ( $Q_{15}F_{25}L_{61}$ ), corresponds to Unit I at Site 974 ( $Q_{19}F_{22}L_{59}$ ), and his upper Oligocene to lower Miocene quartzolithic petrofacies ( $Q_{54}F_{10}L_{36}$ ) corresponds to Unit I at Sites 977, 978, and 979 and Units II and III at Site 976 ( $Q_{51-57}F_{(2-9)}L_{(38-41)}$ ).

## SUMMARY AND CONCLUSIONS

Submarine canyon and onshore drainage patterns suggest that the most likely source of Pleistocene sand-sized sediment at Site 974 was the Tiber River drainage basin in central Italy, where a Pleistocene volcanic field is superimposed on Apennine orogenic rocks. In contrast, the Miocene synrift sand in Unit III may have been derived from local basement highs. The quartzolithic composition and preponderance of metamorphic and sedimentary lithic debris in sand samples from Unit II at Site 976, Unit I at Sites 977 and 978, and Unit I at Site 979 is consistent with derivation from metamorphic rocks and sedimentary cover sequences that crop out in the Betic Cordillera of southern Spain (976–978) and the Rif of Northern Africa (979); the sedimentary to metamorphic lithic fragment ratios in these samples reflect the relative proportion of metamorphic and sedimentary rocks exposed in onshore source terranes. In contrast, the source of the few quartzose Pleistocene sands at Site 976 was likely the Flysch Trough Units that crop out near Gibraltar. The significant volcanic component in certain intervals at Sites 976 (late Miocene) and 977 (early Pliocene to Miocene) is consistent with widespread volcanic activity during basin development. In general, mean sand detrital modes for sand subgroups from both the Alboran and Tyrrhenian Basin sites plot in the Recycled Orogen and Magmatic Arc compositional fields of Dickinson et al. (1983), reflecting the hybrid tectonic histories of these basins.

## ACKNOWLEDGMENTS

This project was supported by a grant to Marsaglia from the National Science Foundation and Joint Oceanographic Institutions administered by the Texas A&M Research Foundation. Petrographic data were collected for this study as part of research for an M.S. thesis by Latter (Sites 976–979 and beach sands) and an undergraduate research project by Cline (Site 974) who was supported by the AMP (Alliance for Minority Participation) program at the University of Texas El Paso. We thank Menchu Comas and an anonymous reviewer for their helpful comments.

## REFERENCES

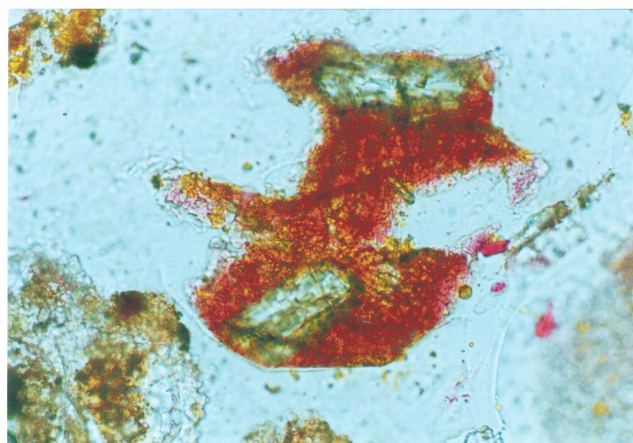
- Alonso, B., and Maldonado, A., 1992. Plio-Quaternary margin growth patterns in a complex tectonic setting: northeastern Alboran Sea. *Geo-Mar. Lett.*, 12:137–143.
- Beccaluva, L., Bonatti, E., Dupuy, G., Ferrara, F., Innocenti, F., Lucchini, F., Macera, P., Petrini, R., Rossi, P.L., Serri, G., Seyler, M., and Siena, F., 1990. Geochemistry and mineralogy of volcanic rocks from ODP Sites 650, 651, 655, and 654 in the Tyrrhenian Sea. In Kastens, K.A., Mascle, J., et al., *Proc. ODP, Sci. Results*, 107: College Station, TX (Ocean Drilling Program), 49–74.
- Bellon, H., Bordet, P., and Montecat, C., 1983. Le magmatisme néogène des Cordillères bétiques (Espagne): chronologie et principaux caractères géochimiques. *Bull. Soc. Geol. Fr.*, Ser. 7, 25:205–218.
- Bellotti, P., Milli, S., Tortora, P., and Valeri, P., 1995. Physical stratigraphy and sedimentology of the late Pleistocene-Holocene Tiber Delta depositional sequence. *Sedimentology*, 42:617–634.
- Bellotti, P., Tortora, P., and Valeri, P., 1986. Sedimentological and morphological features of the Tiber Delta. *Int. Sediment. Congr.*, 12.
- Borsetti, A.M., Curzi, P.V., Landuzzi, V., Mutti, M., Ricci Lucchi, F., Sartori, R., Tomadin, L., and Zuffa, G.G., 1990. Messinian and pre-Messinian sediments from ODP Leg 107 Sites 652 and 654 in the Tyrrhenian Sea: sedimentologic and petrographic study and possible comparisons with Italian sequences. In Kastens, K.A., Mascle, J., et al., *Proc. ODP, Sci. Results*, 107: College Station, TX (Ocean Drilling Program), 169–186.
- Bufo, E., Sanz de Galdeano, C., and Urdias, A., 1995. Seismotectonics of the Ibero-Maghrebian region. *Tectonophysics*, 248:247–261.
- Carter, T.G., Flanagan, J.P., Jones, C.R., Marchant, F.L., Murchison, R.R., Rebman, J.H., Sylvester, J.C., and Whitney, J.C., 1972. A new bathymetric chart and physiography of the Mediterranean Sea. In Stanley, D.J. (Ed.), *The Mediterranean Sea: a Natural Sedimentation Laboratory*: Stroudsburg, PA (Dowden, Hutchinson, and Ross), 1–23.
- Chalouan, A., and Michard, A., 1990. The Ghomarides nappes, Rif coastal range, Morocco: a variscan ship in the Alpine beds. *Tectonics*, 9:1565–1583.
- Comas, M.C., García-Dueñas, V., and Jurado, M.J., 1992. Neogene tectonic evolution of the Alboran Basin from MCS data. *Geo-Mar. Lett.*, 12:157–164.
- Comas, M.C., Zahn, R., Klaus, A., et al., 1996. *Proc. ODP, Init. Repts.*, 161: College Station, TX (Ocean Drilling Program).
- Comas, M.C., Zahn, R., Klaus, A., and ODP Leg 161 Scientific Party, 1996. Las perforaciones del ODP-Leg 161 en el Mediterráneo Occidental. *Geogaceta*, 20:408–411.
- Critelli, S., 1993. Sandstone detrital modes in the Paleogene Liguride Complex, accretionary wedge of the Southern Apennines (Italy). *J. Sediment. Petrol.*, 63:464–476.
- Dickinson, W.R., 1970. Interpreting detrital modes of graywacke and arkose. *J. Sediment. Petrol.*, 40:695–707.
- Dickinson, W.R., Beard, L.S., Brakenridge, G.R., Erjavec, J.L., Ferguson, R.C., Inman, K.F., Knepp, R.A., Lindberg, F.A., and Ryberg, P.T., 1983. Provenance of North American Phanerozoic sandstones in relation to tectonic setting. *Geol. Soc. Am. Bull.*, 94:222–235.
- Fernandez, J.R., and Sanz de Galdeano, C., 1992. Onshore Neogene stratigraphy in the North of the Alboran Sea (Betic Internal Zones): paleogeographic implications. *Geo-Mar. Lett.*, 12:123–128.
- García-Dueñas, V., Balanya, J.C., and Martínez-Martínez, J.M., 1992. Miocene extensional detachments in the outcropping basement of the northern Alboran basin (Betics) and their tectonic implications. *Geo-Mar. Lett.*, 12:88–95.
- Goffé, B., Michard, A., García-Dueñas, V., González Lodeiro, F., Monié, P., Campos, J., Galindo-Zaldívar, J., Jabaloy, A., Martínez-Martínez, J.M., and Simancas, F., 1989. First evidence of high-pressure, low-temperature metamorphism in the Alpujarride nappes, Betic Cordilleras (S.E. Spain). *Eur. J. Mineral.*, 1:139–142.
- Hernandez, J., de Larouzière, F.D., Bolze, J., and Bordet, P., 1987. Le magmatisme néogène bético-rifain et le couloir de décrochement trans-Alboran. *Bull. Soc. Geol. Fr.*, 3:257–267.
- Horvath, F., and Berckhemer, H., 1982. Mediterranean back arc basins. In Berckhemer, H., and Hsü, K.J. (Eds.), *Alpine-Mediterranean Geodynamics*. Ber. Inst. Meteorol. Geophys. Univ. Frankfurt/Main, Geodyn. Ser., 7:141–173.
- Huang, T.-C., and Stanley, D.J., 1972. Western Alboran Sea: sediment dispersal, ponding and reversal of currents. In Stanley, D.J. (Ed.), *The Mediterranean Sea: a Natural Sedimentation Laboratory*: Stroudsburg, PA (Dowden, Hutchinson, and Ross), 521–559.
- Ingersoll, R.V., Bullard, T.F., Ford, R.L., Grimm, J.P., Pickle, J.D., and Sares, S.W., 1984. The effect of grain size on detrital modes: a test of the Gazi-Dickinson point-counting method. *J. Sediment. Petrol.*, 54:103–116.
- Jolivet, L., Daniel, J.M., Truffert, C., and Goffé, B., 1994. Exhumation of deep crustal metamorphic rocks and crustal extension in arc and back-arc regions. *Lithos*, 33:3–30.
- Kairo, S., Suttner, L.J., and Dutta, P.K., 1993. Variability in sandstone composition as a function of depositional environment in coarse-grained delta system. In Johnsson, M.J., and Basu, A. (Eds.), *Processes Controlling the Composition of Clastic Sediments*: Spec. Pap.—Geol. Soc. Am., 284:41–65.
- Kastens, K., and Mascle, J., 1990. The geological evolution of the Tyrrhenian Sea: an introduction to the scientific results of ODP Leg 107. In Kastens, K.A., Mascle, J., et al., *Proc. ODP, Sci. Results*, 107: College Station, TX (Ocean Drilling Program), 3–26.

- Kastens, K.A., Mascle, J., Auroux, C., et al., 1987. *Proc. ODP, Init. Repts.*, 107: College Station, TX (Ocean Drilling Program).
- Latter, K.K., 1998. Sand provenance within the Alboran Sea [M.S. thesis]. Univ. Texas, El Paso.
- Maldonado, A., Campillo, A.C., Mauffret, A., Alonso, B., Woodside, J., and Campos, J., 1992. Alboran Sea late Cenozoic tectonic and stratigraphic evolution. *Geo-Mar. Lett.*, 12:179–186.
- Mantovani, E., Albarello, D., Tamburelli, C., and Barbucci, D., 1996. Evolution of the Tyrrhenian Basin and surrounding regions as a result of the Africa-Eurasia convergence. *J. Geodyn.*, 21:35–72.
- Marsaglia, K.M., García y Barragán, J.C., Padilla, I., and Milliken, K.L., 1996. Evolution of the Iberian passive margin as reflected in sand provenance. In Whitmarsh, R.B., Sawyer, D.S., Klaus, A., and Masson, D.G. (Eds.), *Proc. ODP, Sci. Results*, 149: College Station, TX (Ocean Drilling Program), 269–280.
- Marsaglia, K.M., and Ingersoll, R.V., 1992. Compositional trends in arc-related, deep-marine sand and sandstone: a reassessment of magmatic-arc provenance. *Geol. Soc. Am. Bull.*, 104:1637–1649.
- Marsaglia, K.M., Ingersoll, R.V., and Packer, B.M., 1992. Tectonic evolution of the Japanese Islands as reflected in modal compositions of Cenozoic forearc and backarc sand and sandstone. *Tectonics*, 11:1028–1044.
- Marsaglia, K.M., and Tazaki, K., 1992. Diagenetic trends in Leg 126 sandstones. In Taylor, B., Fujioka, K., et al., *Proc. ODP, Sci. Results*, 126: College Station, TX (Ocean Drilling Program), 125–138.
- McCoy, F.W., and Cornell, W., 1990. Volcaniclastic sediments in the Tyrrhenian Basin. In Kastens, K.A., Mascle, J., et al., *Proc. ODP, Sci. Results*, 107: College Station, TX (Ocean Drilling Program), 291–305.
- Morel, J.L., and Meghraoui, M., 1996. Goringe-Alboran-Tell tectonic zone: a transpression system along the Africa-Eurasia plate boundary. *Geology*, 24:755–758.
- Platt, J.P., and Vissers, R.L.M., 1989. Extensional collapse of thickened continental lithosphere: a working hypothesis for the Alboran Sea and Gibraltar Arc. *Geology*, 17:540–543.
- Rehault, J.P., Mascle, J., Fabbri, A., Moussat, E., and Thommeret, M., 1987a. The Tyrrhenian Sea before Leg 107. In Kastens, K.A., Mascle, J., Auroux, C., et al., *Proc. ODP, Init. Repts.*, 107: College Station, TX (Ocean Drilling Program), 9–36.
- Rehault, J.P., Moussat, E., and Fabri, A., 1987b. Structural evolution of the Tyrrhenian backarc basin. *Mar. Geol.*, 74:123–150.
- Sartori, R., Mascle, G., and du Chaffaut, S.A., 1987. A review of Circum-Tyrrhenian regional geology. In Kastens, K.A., Mascle, J., Auroux, C., et al., *Proc. ODP, Init. Repts.*, 107: College Station, TX (Ocean Drilling Program), 37–64.
- Savelli, C., 1988. Late Oligocene to Recent episodes of magmatism in and around the Tyrrhenian Sea: implications for the processes of opening in a young inter-arc basin of intra-orogenic (Mediterranean) type. *Tectonophysics*, 146:163–181.
- Sedimentation Seminar, 1988. Comparative petrographic maturity of river and beach sand, and origin of quartz arenites. *J. Geol. Educ.*, 36:79–87.
- Selli, R., 1985. Tectonic evolution of the Tyrrhenian Sea. In Stanley, D.J., and Wezel, F.-C. (Eds.), *Geological Evolution of the Mediterranean Basin*: New York (Springer-Verlag), 131–151.
- Shipboard Scientific Party, 1973. Western Alboran Basin Site 121. In Ryan, W.B.F., Hsü, K.J., et al., *Init. Repts. DSDP*, 13: Washington (U.S. Govt. Printing Office), 43–89.
- Stromberg, S.G., and Bluck, B., 1998. Turbidite facies, fluid-escape structures and mechanisms of emplacement of the Oligo-Miocene Aljibe Flysch, Gibraltar Arc, Betics, southern Spain. *Sediment. Geol.*, 115:267–288.
- Vanney, J.-R., and Gennesseaux, M., 1985. Mediterranean seafloor features: overview and assessment. In Stanley, D.J., and Wezel, F.-C. (Eds.), *Geological Evolution of the Mediterranean Basin*: New York (Springer-Verlag), 3–32.
- Wezel, F., 1985. Structural features and basin tectonics of the Tyrrhenian Sea. In Stanley, D.J., and Wezel, F. (Eds.), *Geological Evolution of the Mediterranean Basin*: Berlin (Springer-Verlag), 153–194.

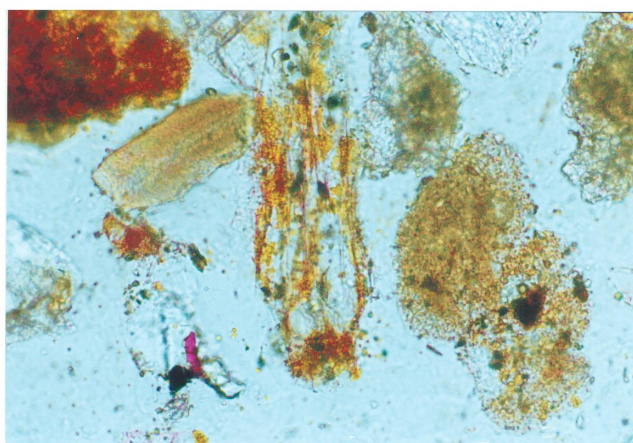
**Date of initial receipt: 12 May 1997**

**Date of acceptance: 14 January 1998**

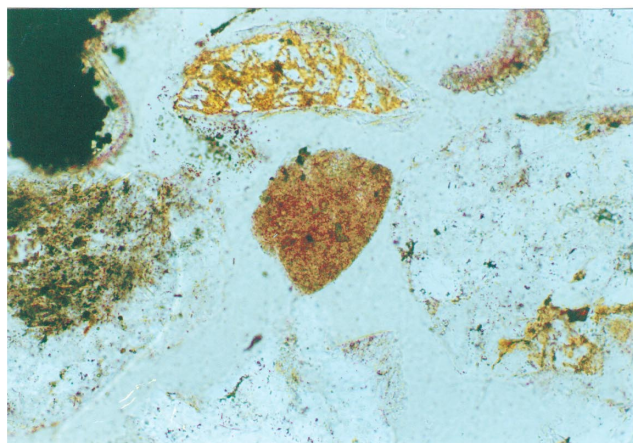
**Ms 161SR-205**



1



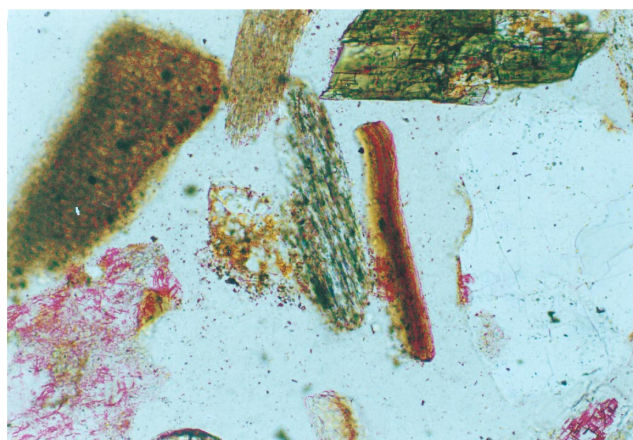
2



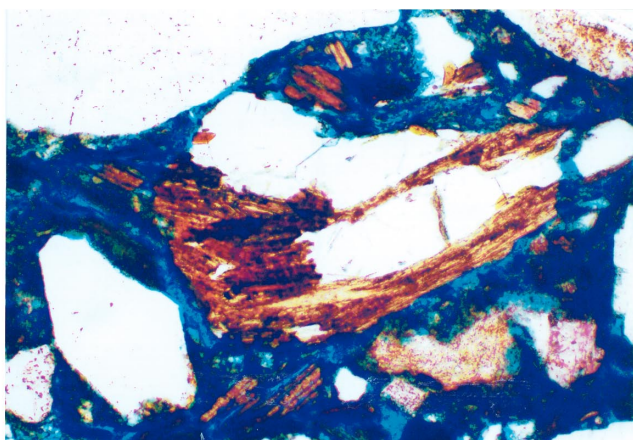
3



4

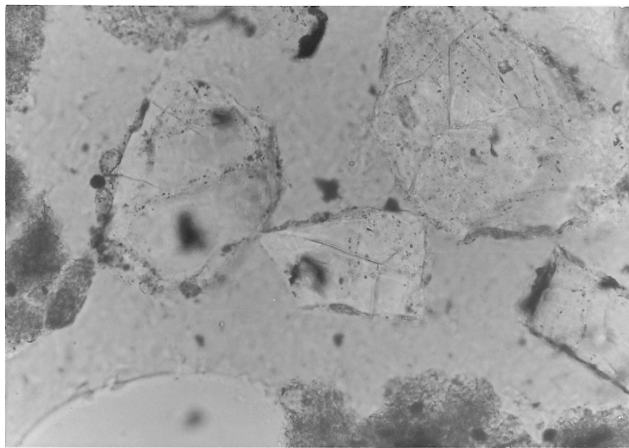


5

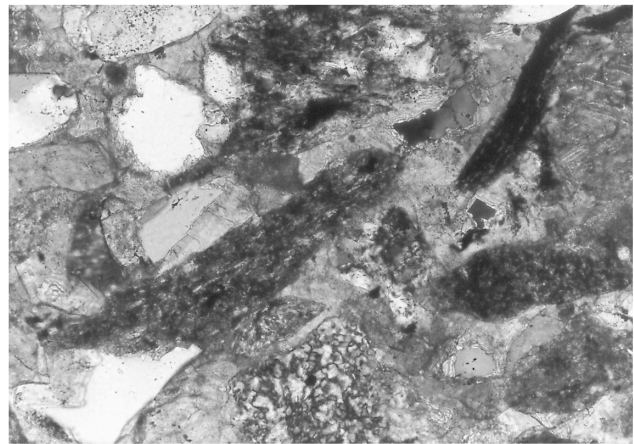


6

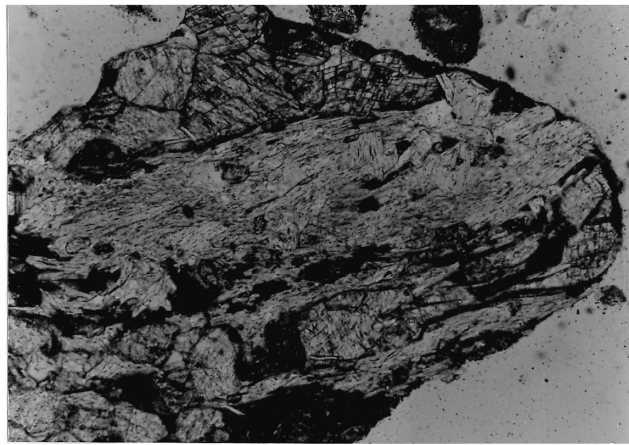
Plate 1. Photomicrographs of sand from Site 974. **1.** Irregular-shaped (vesicular?) brown microlitic-volcanic-lithic fragment. Dark color caused in part by red stain, which reflects a high Ca content of glass. Sample 161-974B-1H-3, 139-140 cm. Scale bar is 0.025 mm. **2.** Stretched pumice (vertical in center). Pumice takes light-pink (Ca) and yellow (K) stain. Sample 161-974B-1H-3, 139-140 cm. Scale bar is 0.05 mm. **3.** Stained potassium feldspar (top center), quartz (bottom center), shale with microquartz vein (left), polycrystalline quartz (right), and bioclastic debris. Sample 161-974B-2H-4, 63-65 cm. Scale bar is 0.05 mm. **4.** Same view as in C, but with crossed nicols. Sample 161-974B-2H-4, 63-65 cm. Scale bar is 0.05 mm. **5.** Red algae fragment (upper left), stained plagioclase (lower left), vertically oriented polycrystalline mica and brown biotite (center), green amphibole (upper right), and quartz (right). Sample 161-974B-2H-4, 63-65 cm. Scale bar is 0.05 mm. **6.** Coarse quartz-biotite schist fragment. Sample 161-974B-22X-CC, 28 cm. Scale bar is 0.2 mm.



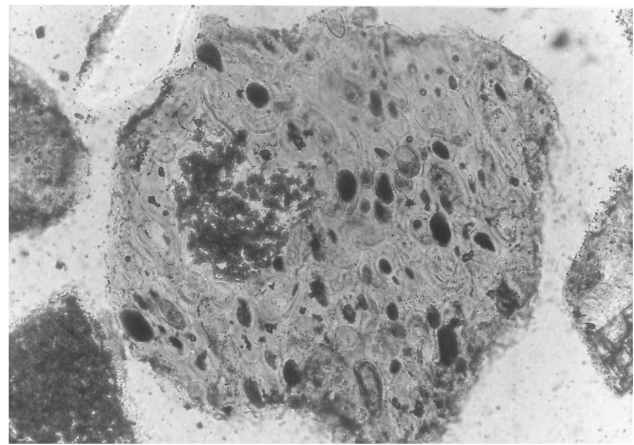
1



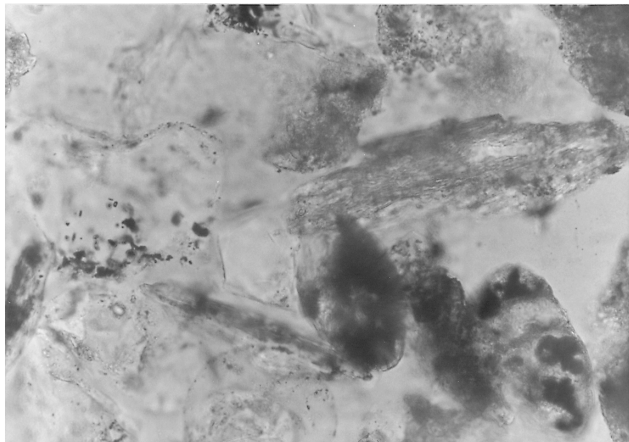
2



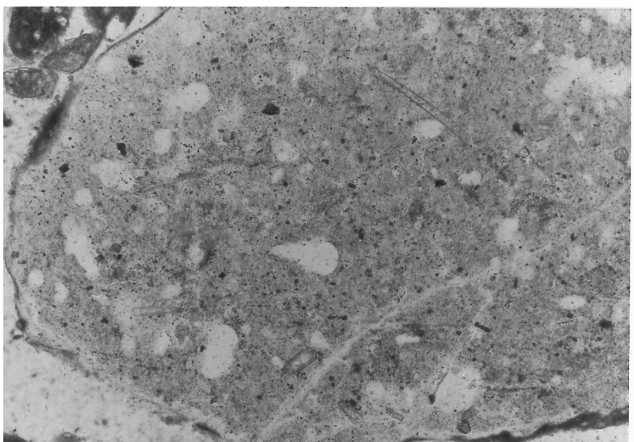
3



4

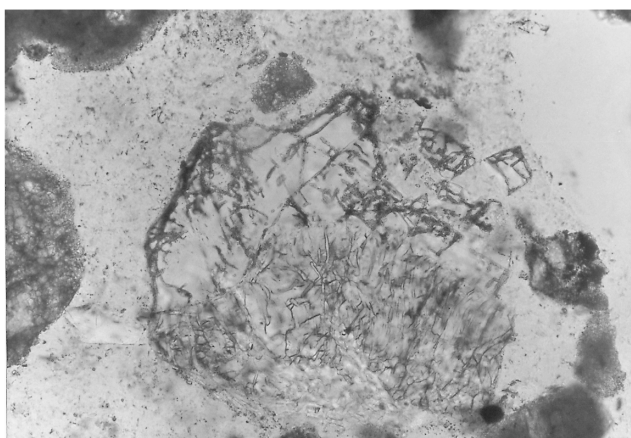


5

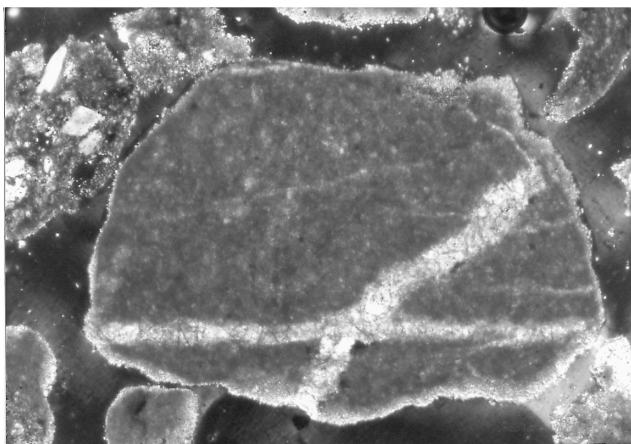


6

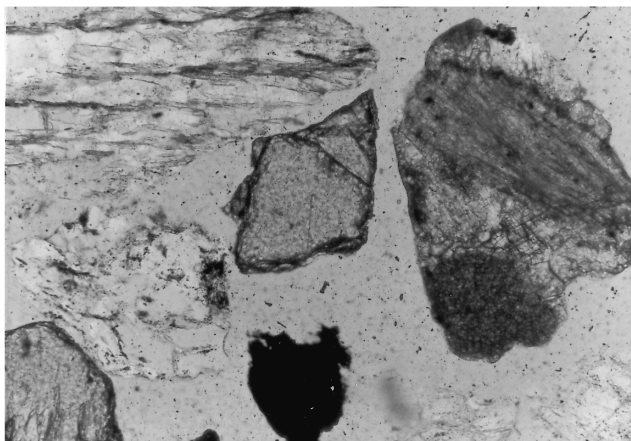
Plate 2. Photomicrographs of sand from Sites 976 and 977. **1.** Quartz grains. Sample 161-976B-3H-1, 72–74 cm. Scale bar is 0.025 mm. **2.** Calcite-cemented sandstone with silty shale/slate fragments, and chert and quartz grains. Crossed nicols. Sample 161-976B-51X-1, 45–47 cm. Scale bar is 0.05 mm. **3.** Calc-schist fragment. Sample 161-976B-72X-CC, 16–18 cm. Scale bar is 0.1 mm. **4.** Vesicular glass (pumice) altered to green clay minerals. Sample 161-976B-72X-CC, 16–18 cm. Scale bar is 0.05 mm. **5.** Quartz, quartz-mica tectonite (schist), foraminifers and mica flake. Sample 161-977A-22X-CC, 19–20 cm. Scale bar is 0.025 mm. **6.** Fragment of fractured, radiolarian-bearing (round and conical white spots) argillaceous chert. Sample 161-977A-57X-CC, 33–34 cm. Scale bar is 0.1 mm.



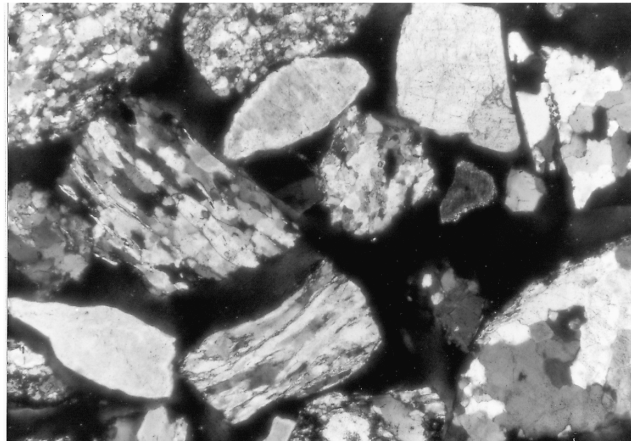
1



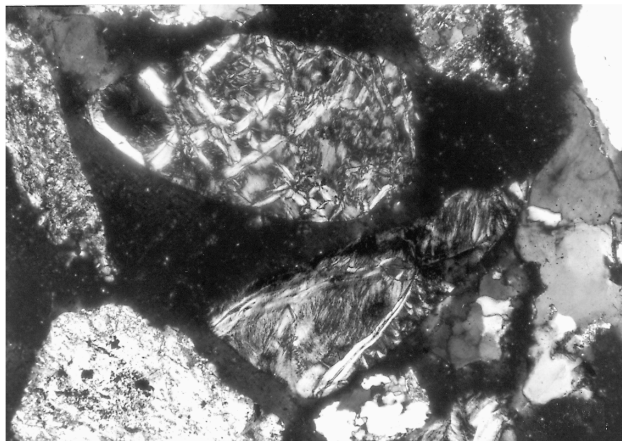
2



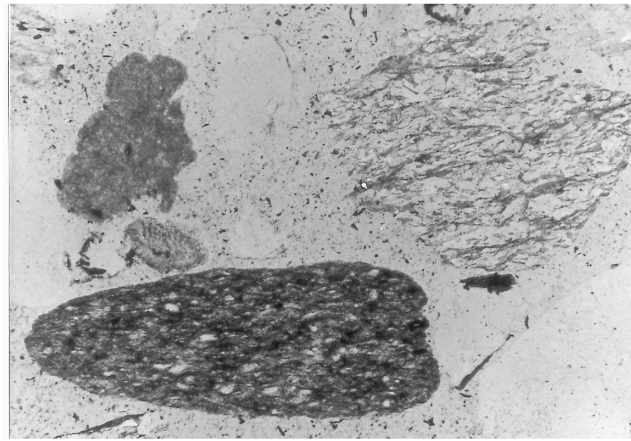
3



4



5



6

Plate 3. Photomicrographs of sand from Site 977 and Spanish beaches. **1.** Granitic or gneissic fragment composed of plagioclase feldspar (bottom of grain) and potassium feldspar (top of grain). Feldspar is etched and stained; Sample 161-977A-57X-CC, 33–34 cm. Scale bar is 0.1 mm. **2.** Micrite sedimentary lithic fragment with carbonate veins. Sample 161-977A-57X-CC, 33–34 cm. Scale bar is 0.1 mm. **3.** Quartz-mica tectonite fragments (top and center on left), garnet (center), and carbonate lithic fragment (right). Beach sample (#3) taken near Almería. Scale bar is 0.1 mm. **4.** Quartz-mica tectonite fragments and monocrystalline and polycrystalline quartz fragments. Beach sample (#5) taken between Almería and Malaga. Scale bar is 0.2 mm. **5.** Serpentinite fragments (center). Crossed nicols. Beach sample (#9) taken west of Malaga. Scale bar is 0.1 mm. **6.** Silty shale fragment (lower left), limestone fragment (upper left), quartz-mica tectonite fragment (upper right) and quartz grains. Beach sample (#6) taken west of Malaga. Scale bar is 0.1 mm.